Incorporation of minor and trace elements into cultured brachiopods: Implications for proxy application with new insights from a biomineralisation model

Hana Jurikova [a,b], Mats Ippach [a], Volker Liebetrau [a], Marcus Gutjahr [a], Stefan Krause [a], Sebastian Büsse [c], Stanislav N. Gorb [c], Daniela Henkel [a], Claas Hiebenthal [a], Mark Schmidt [a], Thomas Leipe [d], Jürgen Laudien [e], Anton Eisenhauer [a]

[a] *GEOMAR Helmholtz-Zentrum für Ozeanforschung Kiel, Wischhofstr. 1-3, 24148 Kiel, Germany*
[b] *Deutsche GeoForschungsZentrum GFZ – Helmholtz-Zentrum Potsdam, Telegrafenberg, 14473 Potsdam, Germany*
[c] *Zoologisches Institut, Christian-Albrechts-University Kiel, Am Botanischen Garten 1-9, 24118 Kiel, Germany*
[d] *Leibniz-Institut für Ostseeforschung Warnemünde, Seestr. 15, 18119 Rostock, Germany*
[e] *Alfred-Wegener-Institut Helmholtz-Zentrum für Polar- und Meeresforschung, Am Handelshafen 12, 27570 Bremerhaven, Germany*

Abstract

Brachiopods present a key fossil group for Phanerozoic palaeo-environmental and palaeo-oceanographical reconstructions, owing to their good preservation and abundance in the geological record. Yet to date, hardly any geochemical proxies have been calibrated in cultured brachiopods and only little is known on the mechanisms that control the incorporation of various key elements into brachiopod calcite. To evaluate the feasibility and robustness of multiple Element/Ca ratios as proxies in brachiopods, specifically Li/Ca, B/Ca, Na/Ca, Mg/Ca, Sr/Ca, Ba/Ca, as well as Li/Mg, we cultured *Magellania venosa*, *Terebratella dorsata* and *Pajaudina atlantica* under controlled experimental settings over a period of more than two years with closely monitored ambient conditions, carbonate system parameters and elemental composition of the culture medium. The experimental setup comprised of two control aquariums ($pH_0 = 8.0$ and 8.15, $T = 10\ °C$) and treatments where $pCO_2 - pH$ ($pH_1 = 7.6$ and $pH_2 = 7.35$), temperature ($T = 16\ °C$) and chemical composition of the culture medium were manipulated. Our results indicate that the incorporation of Li and Mg is strongly influenced by temperature, growth effects as well as carbonate chemistry, complicating the use of Li/Ca, Mg/Ca and Li/Mg ratios as straightforward reliable proxies. Boron partitioning varied greatly between the treatments, however without a clear link to carbonate system parameters or other environmental factors. The partitioning of both Ba and Na varied between individuals, but was not systematically affected by changes in the ambient conditions. We highlight Sr as a potential proxy for DIC, based on a positive trend between Sr partitioning and carbonate chemistry in the culture medium. To explain the observed dependency and provide a quantitative framework for exploring elemental variations, we devise the first biomineralisation model for brachiopods, which results in a close agreement between modelled and measured Sr distribution coefficients. We propose that in order to sustain shell growth under increased DIC, a decreased influx of Ca^{2+} to the calcifying fluid is necessary, driving the preferential substitution of Sr^{2+} for Ca^{2+} in the crystal lattice. Finally, we conducted micro-computed tomography analyses of the shells grown in the different experimental treatments. We present pore space – punctae – content quantification that indicates that shells built

under increased environmental stress, and in particular elevated temperature, contain relatively more pore space than calcite, suggesting this parameter as a potential novel proxy for physiological stress and even environmental conditions.

1. INTRODUCTION

Brachiopods present an advantageous archive for inferring past global changes, owing to their good preservation and high abundance in the fossil record. They have been increasingly employed for reconstructing past changes of Phanerozoic seawater chemistry and climate state (e.g. Veizer et al., 1999; Farkaš et al., 2007; Brand et al., 2012, Vollstaedt et al., 2014; Garbelli et al., 2019). However, to date, geochemical proxy relationships in brachiopods have been hardly examined under controlled conditions (Jurikova et al., in press-a) and only little is known about the factors that govern the distribution of key elements between the shell and seawater. Culturing experiments, where the newly grown calcite is precipitated within a strictly controlled medium of known chemical composition, are fundamental for understanding the controls on incorporation of major and trace elements into the biomineral. Furthermore, such experiments permit us to reduce the uncertainties related to the interpretation of palaeo-environmental and palaeo-climatic records as well as offer new insights on organisms' biomineralisation strategies.

Presently, the knowledge on Element/Ca ratios in brachiopods is based on variations observed in modern shells (Ullmann et al., 2017), but mostly limited to studies focused on the distribution of single elements in the distinct shell layers (primary vs. secondary, and when applicable tertiary) and microstructures (Pérez-Huerta et al., 2008; Cusack et al., 2008; Romanin et al., 2018; Gaspard et al., 2018; Rollion-Bard et al., 2019). Articulate brachiopods predominantly secrete a low-Mg calcite shell, which in terebratellids typically consists of a relatively thin outer primary layer built of acicular calcite and a thicker innermost secondary layer consisting of calcite fibres, traversed by characteristic pores – punctae (e.g. Pérez-Huerta et al., 2009; Roda et al., 2019). In two-layered brachiopods, the secondary layer presents the optimal target for geochemical analyses, due to minimal kinetic effects and better resistance to diagenetic alterations (e.g. Romanin et al., 2018; Ye et al., 2019). Mg/Ca is amongst the most studied Element/Ca ratios and a well-established temperature proxy in foraminifera (Nürnberg et al., 1996). In brachiopods, Mg/Ca has been proposed to reflect seawater temperature (Brand et al., 2003; Pérez-Huerta et al., 2008; Butler et al., 2015), but also appears to respond to physiological processes (e.g. Buening and Carlson, 1992; England et al., 2006; Cusack et al., 2008; Jurikova et al., in press-a; Kocsis et al., 2020). In addition, similar to other calcifiers, Sr/Ca and Li/Ca ratios have been suggested to record temperature trends in brachiopods (Delaney et al., 1989; Carpenter and Lohmann, 1992), but also seem to be influenced by other parameters including seawater and carbonate chemistry, growth and/or

physiological effects. Furthermore, Li/Mg has over the past years emerged as a new promising tool for inferring seawater temperatures from coral skeletons and even foraminifera (Bryan and Marchitto, 2008; Case et al., 2010; Hathorne et al., 2013a, 2013b; Raddatz et al., 2013; Montagna et al., 2014; Fowell et al., 2016). While the application of Li/Mg has been largely successful in corals secreting aragonite, this may not be directly comparable to the calcitic brachiopods and demands assessment. The B/Ca ratio in foraminifera, on the other hand, has been reported to record seawater carbonate chemistry, and in particular carbonate ion concentrations (Yu et al., 2007; Allen and Hönisch, 2012; Henehan et al., 2015; Rae et al., 2011), but its key controls are yet to be evaluated in brachiopods. Na/Ca or Ba/Ca ratios in foraminifera have been found to depend on the concentration of the respective element in seawater and were thus suggested as potential proxies for salinity (e.g. Mezger et al., 2016) or alkalinity (e.g. de Nooijer et al., 2017), respectively. Similarly, in brachiopods, Na/Ca appears to be positively correlated to salinity (Rollion-Bard et al., 2019), however, the utility of Ba/Ca is yet to be examined in detail. Taken altogether, although the number of studies dealing with geochemistry of brachiopods has been on the rise over the past years, clearly wide gaps still exist in our understanding of the controls on the incorporation of multiple key elements and their potential as proxies in brachiopods. Particularly poorly constrained is the partitioning of elements between brachiopod calcite and seawater, which we examine in detail in this study.

Here, we present chemical analyses of brachiopods – predominantly *Magellania venosa* (Dixon, 1789), but limited results from *Terebratella dorsata* (Gmelin, 1791) of the family Terebratellidae are also included – cultured under different experimental conditions. The culturing of *Pajaudina atlantica* (family Thecideidae) is also mentioned. We explore multiple Element/Ca ratios, specifically Li/Ca, B/Ca, Na/Ca, Mg/Ca, Sr/Ca, Ba/Ca, as well as Li/Mg ratio and their underlying controls on incorporation into the calcite and link to environmental parameters. Additionally, we also consider the impact of environmental changes on the shell microstructure and examine its application as a potential proxy. Finally, we present the first biomineralisation model for brachiopods that offers a simple quantitative framework for exploring the elemental variations and provides new insights into brachiopod calcification mechanisms.

2. MATERIALS AND METHODS

2.1. Brachiopod culturing experiments

A detailed description of the materials and methods is provided in Jurikova et al. (in press-a), however we reiterate

the key points here. In brief, three different brachiopod species were cultured for more than two years in a climatically controlled laboratory (of the KIMOCC – Kiel Marine Organism Culture Center) at GEOMAR in Kiel, Germany (Fig. 1). The temperate brachiopod *Magellania venosa* along with few individuals of *Terebratella dorsata* were collected from Comau Fjord in Chilean Patagonia, and the warm-water dwelling *Pajaudina atlantica* were sampled from La Palma in the Canary Islands. All brachiopods were first acclimatized to the laboratory environment. Prior to the start of the experimental treatments all organisms were labelled using a fluorescent calcein dye to distinguish the newly grown shell increments. Artificial seawater was used as a culture medium, prepared by mixing of commercial Tropic Marin Pro-Reef sea-salt with deionised water until desired salinity and elemental concentrations were achieved (Atkinson and Bingman, 1998). In total, nine different culturing treatments were used for the entire experiment (Table 1). The experimental setup for *P. atlantica* comprised a control, high and low temperature, and various acidification treatments. In this study we principally focus on the setup with *M. venosa,* which consisted of a control, temperature and acidification experiments and an additional treatment where the Mg/Ca of seawater was modified. The temperature, salinity and pH in the control treatments simulated typical natural conditions for each species, and were not directly manipulated during the culturing (Table 1). We noted that the total alkalinity was slightly elevated in the control treatments in contrast to the typical natural conditions. Depending on the treatment, the seawater temperature was maintained constant using either heaters or coolers (Aqua Medic, Germany) (Table 1). The Mg/Ca ratio of seawater was controlled by regular addition of calcium chloride ($CaCl_2$) into the seawater. Acidification was mediated by continuous bubbling of CO_2-enriched air through an air stone. Due to the reduced air circulation in our enclosed climate laboratory, the pCO_2 was slightly elevated (600 µatm) in the room air as well as in the control and the other non-acidification treatments with respect to the natural atmospheric conditions (app. 410 µatm, NOAA, 2019), however the pH was representative

of normal seawater conditions (pH = 8.0 to 8.15 ± 0.05). The CO_2 experimental period may be split into two phases or periods: the first phase (P1) took place between August 2016 and April 2017; the second phase (P2) lasted from April 2017 until July 2017. The two different time-phases principally refer to the intensity of the acidification treatments. During P1 the enriched CO_2 partial pressure was maximum 2000 µatm; for the P2 the pCO_2 was elevated from initial 1500 µatm to 4000 µatm in the aquarium B1, and from 2000 µatm to 4000 µatm in the aquarium C3 (Table 1). While no other parameters or aquarium conditions were manipulated during P2, we noted that the carbonate chemistry of the control treatments slightly differed between P1 and P2, presumably due to brachiopod sampling, hence the removal of a calcifying organism from the tank. Samples for the present study were harvested in February and July 2017, and final culturing experiments terminated in June 2018.

For the monitoring of the conditions in the cultures, all aquariums were equipped with automated sensors for continuous measurements of salinity (Conductivity Electrode), temperature (Temperature Sensor Aquarium for *P. atlantica* and Temperature Sensor Pond for *M. venosa* aquariums) and pH (pH-Electrode) connected to a GHL ProfiLux aquarium computer 3.1 T eX (GHL, Kaiserslautern, Germany) for data storing, and were validated against manual measurements several times per week. An optical membrane-inlet CO_2 sensor (CONTROS HydroC® underwater CO_2 sensor; Kongsberg Maritime Contros GmbH, Kiel, Germany) calibrated for a pCO_2 range of 200–6000 µatm (with accuracy ∼1% of reading) was used for continuous monitoring of the pCO_2 in the aquariums as well as the CO_2 in the room air. Seawater from all brachiopod-culturing aquariums, reservoir tanks, and the deionized water source was routinely sampled and analysed for elemental content, total alkalinity (TA) and total dissolved inorganic carbon (DIC). Carbonate system parameters were determined as described previously (Jurikova et al., in press-a) and the calcite saturation state (Ω_{cal}) was calculated according to Zeebe and Wolf-Gladrow (2001). Seawater samples for elemental analyses were
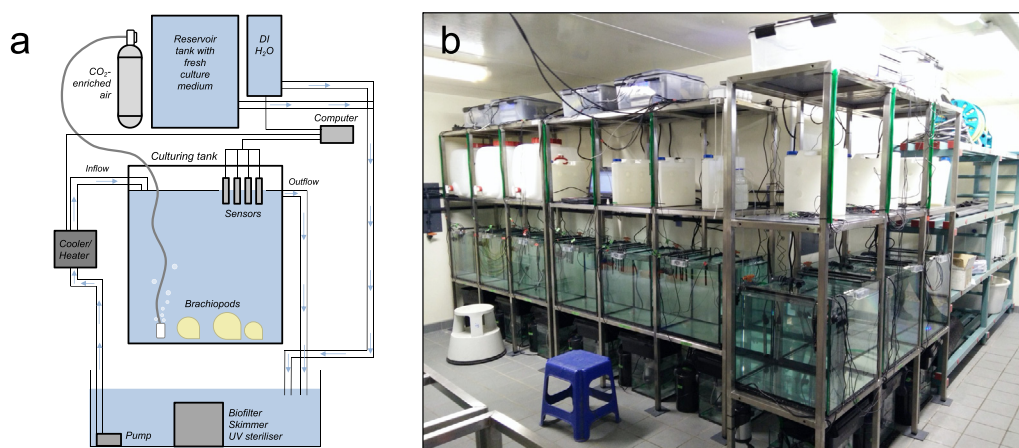

Fig. 1. (a) A schematic diagram of our culturing tank with CO_2-enriched air source; (b) a photo of the complete experimental setup with nine culturing tanks at GEOMAR (KIMOOC), Kiel. DI H₂O - deionised water.

Table 1
Summary of the experimental culturing settings, seawater and carbonate system parameters ($\pm 1\sigma$ long-term variations throughout the duration of the corresponding treatments). Temperature, pCO_2, pH, TA and DIC were measured; HCO_3^- and CO_3^{2-} calculated from pH and TA, and Ω_{cal} determined as given in Eq. (6). Throughout the culturing salinity and temperature were maintained constant. For phase 2 (P2) CO_2 partial pressure was increased from initial 1500 µatm to 4000 µatm in the aquarium B1, and from 2000 µatm to 4000 µatm in the aquarium C3 resulting in changes of the carbonate chemistry. In the aquarium C1, the Mg/Ca ratio of seawater was modified by addition of calcium chloride ($CaCl_2$) and was lowered from normal value of 4.8 ± 0.2 mol/mol prior to the start of experimental treatments to 3.6 ± 0.2 mol/mol during both culturing phases from August 2016 until July 2017. *Note: Tank including few individuals of *T. dorsata* individuals cultured along with *M. venosa*.

Aq. No.	Treatment	ID	Species	Sal.	T [°C]	pCO_2 [µatm]	pH	TA [mmol/l]	DIC [mmol/l]	HCO_3^- [mmol/l]	CO_3^{2-} [mmol/l]	Ω_{cal}
				± 0.05	± 1	$\pm 10\%$	± 0.05	± 0.3	$\pm 12\%$			
Phase 1 (P1): August 2016 − April 2017												
A1	Control	pH_0	*P. atlantica*	36	22	600	8.20	3.2	2.6	2.34	0.37	9.9
A2	Temp. high	T_+	*P. atlantica*	36	25	600	8.20	3.2	2.7	2.27	0.40	13.3
A3	Acid. (pCO_2)	pH_1	*P. atlantica*	36	22	2000	7.70	3.4	2.7	3.05	0.15	4.6
B1	Acid. (pCO_2)	$pH_{1/2}$	*P. atlantica*	36	22	1500	7.80	3.3	3.5	2.88	0.18	4.8
B2	Temp. low	T_-	*P. atlantica*	36	18	600	8.20	3.6	2.6	2.75	0.37	9.0
B3	Temp. high	T_+	*M. venosa*	30	16	600	8.20	3.5	2.6	2.81	0.30	6.9
C1	Mg/Ca	Mg/Ca	*M. venosa*	30	10	600	8.05	2.7	2.8	2.36	0.14	6.3
C2	Control	pH_0	*M. venosa**	30	10	600	8.00	2.3	2.0	2.03	0.11	2.0
C3	Acid. (pCO_2)	pH_1	*M. venosa*	30	10	2000	7.60	2.8	2.7	2.66	0.06	1.1
Phase 2 (P2): April 2017 − July 2017												
A1	Control	pH_0	*P. atlantica*	36	22	600	8.25	3.8	2.6	2.71	0.48	10.4
A2	Temp. high	T_+	*P. atlantica*	36	25	600	8.25	3.3	2.6	2.27	0.45	11.7
A3	Acid. (pCO_2)	pH_1	*P. atlantica*	36	22	2000	7.70	3.3	2.8	2.96	0.15	3.9
B1	Acid. (pCO_2)	$pH_{1/2}$	*P. atlantica*	36	22	4000	7.35	3.5	3.1	3.33	0.07	2.0
B2	Temp. low	T_-	*P. atlantica*	36	18	600	8.20	3.6	2.8	2.75	0.37	10.4
B3	Temp. high	T_+	*M. venosa*	30	16	600	8.20	3.7	2.8	2.97	0.32	7.5
C1	Mg/Ca	Mg/Ca	*M. venosa*	30	10	600	8.05	2.7	2.5	2.36	0.14	6.3
C2	Control	pH_0	*M. venosa**	30	10	600	8.15	2.9	2.9	2.46	0.20	3.5
C3	Acid. (pCO_2)	pH_1	*M. venosa*	30	10	4000	7.35	3.1	3.5	3.01	0.04	0.6

collected in 4 ml vials using syringe filters (28 mm diameter, SFCA membrane, 0.2 μm mesh size), acidified (40 μl concentrated HNO₃ for the total volume of 4 ml), and stored in a refrigerator room until analysis.

2.2. Sample preparation and elemental analyses

For this study, typically 6–7 *M. venosa* individuals were used from each control or acidification tank, 2 *T. dorsata* from the control, and one *M. venosa* specimen from each high temperature and Mg/Ca treatments (see Supplement). All brachiopod shells were first gently rinsed with ultra-pure water (Milli-Q), and then dried over few days on a hotplate at 40 °C in a clean flow hood. Selected growth increments precipitated under specific treatment conditions labelled with calcein (Fig. 2) were subsampled for mini-bulk analyses under binoculars using a precision drill (Proxxon) with dental tips. Altogether approximately 1–3 mg of homogenous CaCO₃ powder was collected in 1.5 ml centrifuge vials. Powder material was oxidatively cleaned following our previously established protocols detailed in Jurikova et al. (in press-a). Finally, each sample was completely dissolved in 0.5 M HNO₃, of which an aliquot of 10% was used to determine the elemental content presented in this study (remaining 90% were used for other isotopic analyses including boron detailed elsewhere). Li, B, Na, Mg, Al, Ca, Mn, Fe, Sr, Cd, Ba, Nd and U content was measured on a Quadrupole ICP-MS (Agilent 7500x) at GEOMAR, Kiel. For the analyses, both standards and samples were diluted to 25 ppm Ca, and a 4-point calibration using multi-elemental standards matching a typical brachiopod matrix was used to convert the counts to concentrations. All elemental ratios were normalised to those of Hathorne et al.

(2013a, 2013b) by matching here measured JCp-1 standards (Okai et al., 2002) to the values reported in Hathorne et al. (2013a, 2013b). The normalisation was carried out as part of the established routine for our laboratory; however, we note that, in general, we did not find any significant differences between our non-corrected values and those of Hathorne et al. (2013a, 2013b), and for most instances the normalisation was on the order of few % and thus within the analytical uncertainties. The long-term external reproducibility RSD (relative standard deviation, 2σ) for the relevant ratios presented in this study was better than 2% for Li/Ca, 3% for B/Ca, 6% for Na/Ca, 2% for Mg/Ca and Sr/Ca, and 4% for Ba/Ca assessed by repeated measurements of carbonate reference materials JCp-1, JCt-1 and an in-house *M. venosa* brachiopod standard MVS-1 (all sample as well as reference material data is available in Supplement).

Filtered and acidified culture medium samples were measured for Li, B, Na, Mg, K, Ca, Sr and Ba content on an ICP-OES (Inductively Coupled Plasma-Optical Emission Spectrometry) Varian 720-ES at GEOMAR, Kiel. The long-term external reproducibility RSD (relative standard deviation, 2σ) for the relevant ratios was better than 3% for Li/Ca, 2% for B/Ca, Na/Ca, Mg/Ca and Sr/Ca, and 4% for Ba/Ca determined by repeated measurements of IAPSO standard seawater (see Supplement for data).

2.3. Partition coefficients

Empirical partition (distribution) coefficients were used to describe the partitioning of elements between the brachiopod calcite and culture medium (artificial seawater). Using measured Element/Ca ratios the partition coefficients $K_{D(X)}$ were calculated as follows:
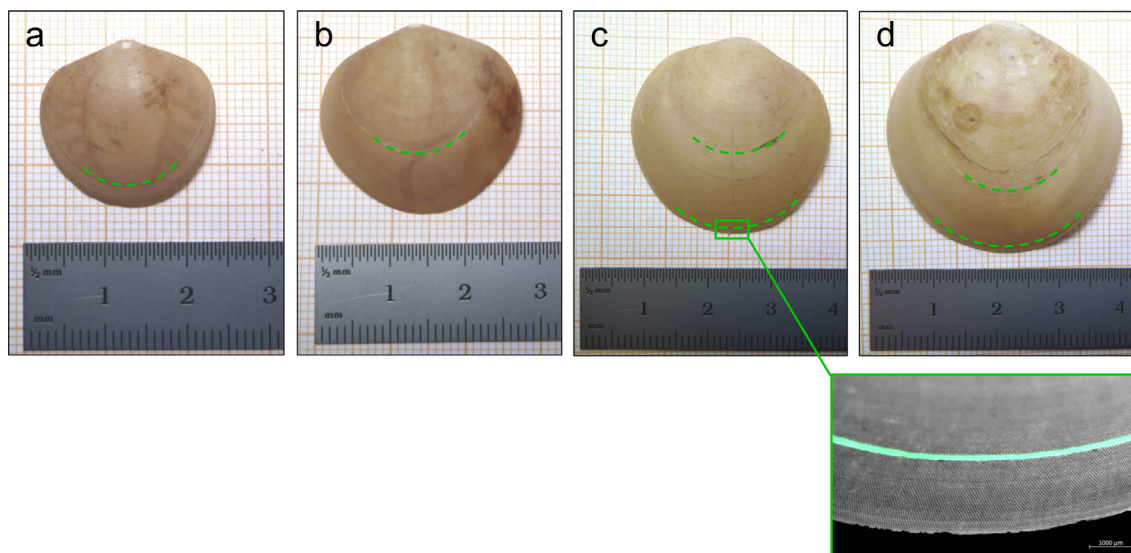

Fig. 2. Examples of *Magellania venosa* specimens used in this study from different culturing treatments: (a) high temperature (aquarium B3); (b) Mg/Ca experiment (C1); (c) control (C2); and (d) acidification (C3) treatments. The dashed green lines indicate the position of calcein marker that allows for distinguishing between shell parts grown in nature and in culture, as detailed in the enlarged microscope image with a fluorescence filter. The control and acidification treatment samples were marked twice as the pCO₂-pH experiment was carried out in two time phases (early moderate acidification (P1) and later extreme acidification phase (P2), as described in Section 2.1). (For interpretation of the references to colour in this figure legend, the reader is referred to the web version of this article.)

$$K_{D(X)} = \frac{\left(\frac{X}{Ca}\right)_{cal}}{\left(\frac{X}{Ca}\right)_{sw}} \qquad (1)$$

where $(X/Ca)_{cal}$ is the measured molar ratio of a given element and Ca in calcium carbonate and $(X/Ca)_{sw}$ is that of seawater, specifically culture medium (see Supplement for data). For convenience all $K_{D(X)}$ values are reported as $K_{D(X)} \times 10^3$. Because boron does not substitute for Ca^{2+} in the $CaCO_3$ crystal lattice but for a CO_3^{2-} group, the B partition coefficient $K_{D(B)}$ was calculated taking into account the selective incorporation of $B(OH)_4^-$ into $CaCO_3$. In seawater, the proportions of the two major boron species $B(OH)_3$ and $B(OH)_4^-$ vary with pH, with $B(OH)_4^-$ being preferentially incorporated into $CaCO_3$ (Hemming et al., 1995):

$$CaCO_3 + B(OH)_4^- \leftrightarrow Ca(HBO_3) + HCO_3^- + H_2O \qquad (2)$$

The apparent partition coefficient $K_{D(B)}$ can then be defined as:

$$K_{D(B)} = \frac{\left[HBO_3^{2-}/CO_3^{2-}\right]_{cal}}{\left[B(OH)_4^-/HCO_3^-\right]_{sw}} = \frac{[B/Ca]_{cal}}{\left[B(OH)_4^-/HCO_3^-\right]_{sw}} \qquad (3)$$

assuming that $CO_3^{2-} \approx Ca^{2+}$.

2.4. Electron microprobe mapping

JEOL JXA 8200 electron (microprobe) analyses were used to map the elemental distribution in shell microstructures. Quantitative elemental maps were generated by wavelength dispersive x-ray spectrometry simultaneously measuring Mg, Ca, Sr, Cl and S following Jurikova et al. (in press-a). Standards (Calcite, Sphalerite, Modern Coral-A2, Dolomite, KANI, Strontianite, VG-2) were measured before and after sample analyses to calculate absolute elemental concentrations.

2.5. µCT analyses

High-resolution X-ray computed tomography (µCT) was carried out using a SkyScan 1172 desktop µCT scanner (Bruker, Kontich, Belgium) at Kiel University. The µCT dataset was reconstructed using the NRecon reconstruction software (Bruker) to eliminate scanning artefacts. Visualization and segmentation was done with AVIZO 9.5 package. Following volume rendering and background subtraction, regions of interest were defined on the scanned shell parts. The sub-volumes were individually segmented using the AVIZO threshold tool to separate brachiopod calcite from pore space – punctae – volume. Total carbonate and punctae void volumes were calculated using the material statistics function of the software. The final punctae content is reported in percent (%) of the shell, by dividing the punctae void volume by the sum of the mineral and void volume.

3. RESULTS

3.1. Culture medium carbonate chemistry

The carbonate chemistry in our aquariums is illustrated in Fig. 3, but prior to discussing the results we briefly reca-pitulate some relevant concepts. In seawater, CO_2 exists in three major inorganic forms: as free aqueous CO_2, bicarbonate HCO_3^- and carbonate ion CO_3^{2-}. The fourth form is carbonic acid H_2CO_3 and is comparatively very minor (up to 0.3% of the $CO_{2(aq)}$). The carbonate species are related by the following equilibriums:

$$CO_{2(aq)} + H_2O \leftrightarrow H_2CO_3 \leftrightarrow HCO_3^- + H^+$$
$$\leftrightarrow CO_3^{2-} + 2H^+ \qquad (4)$$
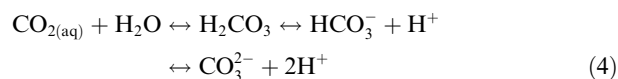
The sum of the dissolved CO_2, HCO_3^- and CO_3^{2-} forms dissolved inorganic carbon (DIC). The total alkalinity (TA) additionally includes boron species:

$$TA \cong \left[HCO_3^-\right] + 2\left[CO_3^{2-}\right] + \left[B(OH)_4^-\right] + [OH^-]$$
$$- [H^+] \; (+ \text{ other minor components}) \qquad (5)$$

Dissolution of CO_2 into seawater decreases the thermodynamic potential for $CaCO_3$ to form, i.e. the saturation state (Ω), described as:

$$\Omega_{cal} = \frac{[Ca^{2+}] \times [CO_3^{2-}]}{K_{sp}^*}, \qquad (6)$$

where K_{sp}^* is the solubility product – in this case calcite – at in situ conditions.

Generally, the carbonate chemistry in most of our culturing tanks was only partially coupled, typically with a close relationship between pH and Ω_{cal}, and pCO$_2$, DIC and TA (Fig. 3). In most of the experimental tanks, pH and Ω_{cal} followed a close exponential fit (Fig. 3a and d), with the exception of two M. venosa treatments, where the chemistry was clearly different – the Mg/Ca and the temperature treatment tanks (Fig. 3d). In the Mg/Ca experiment the pH was comparable to the control treatments, but regular addition of $CaCl_2$ (to purposely decrease the Mg/Ca ratio of culture medium) resulted in considerably higher Ω_{cal} values. Further, the temperature experiment had elevated Ω_{cal} as well as TA values (Fig. 3d–f), likely linked to reduced $CaCO_3$ precipitation rates in the aquarium. Overall, the M. venosa individuals kept in the temperature treatment under thermal stress showed visibly less newly-grown material added at the shell margin (in length, less than a half that seen in M. venosa from the other treatments, see Fig. 2; further details also available in Jurikova et al., in press-a). Taking into account that precipitation of 1 mol of $CaCO_3$ reduces DIC by 1 mol and TA by 2 mol (Zeebe and Wolf-Gladrow, 2001), decreased shell formation in the temperature tank can be expected to more strongly affect the TA compared with the DIC content, and thus could explain why the measured DIC values are within the range of other experimental tanks, but TA is notably elevated (Fig. 3f). In contrast to the M. venosa aquariums, variations in TA and DIC in the P. atlantica treatments were relatively narrow. To a large extent this can be ascribed to the minimal and cryptic new shell growth in all the cultured P. atlantica individuals (Jurikova et al., in press-a). Finally, the DIC content in the culturing tanks was mostly linked to the pCO$_2$ (Fig. 3c and f), although during the later culturing phase P2 DIC was generally higher (in both control and acidification treatments) than during the initial P1.
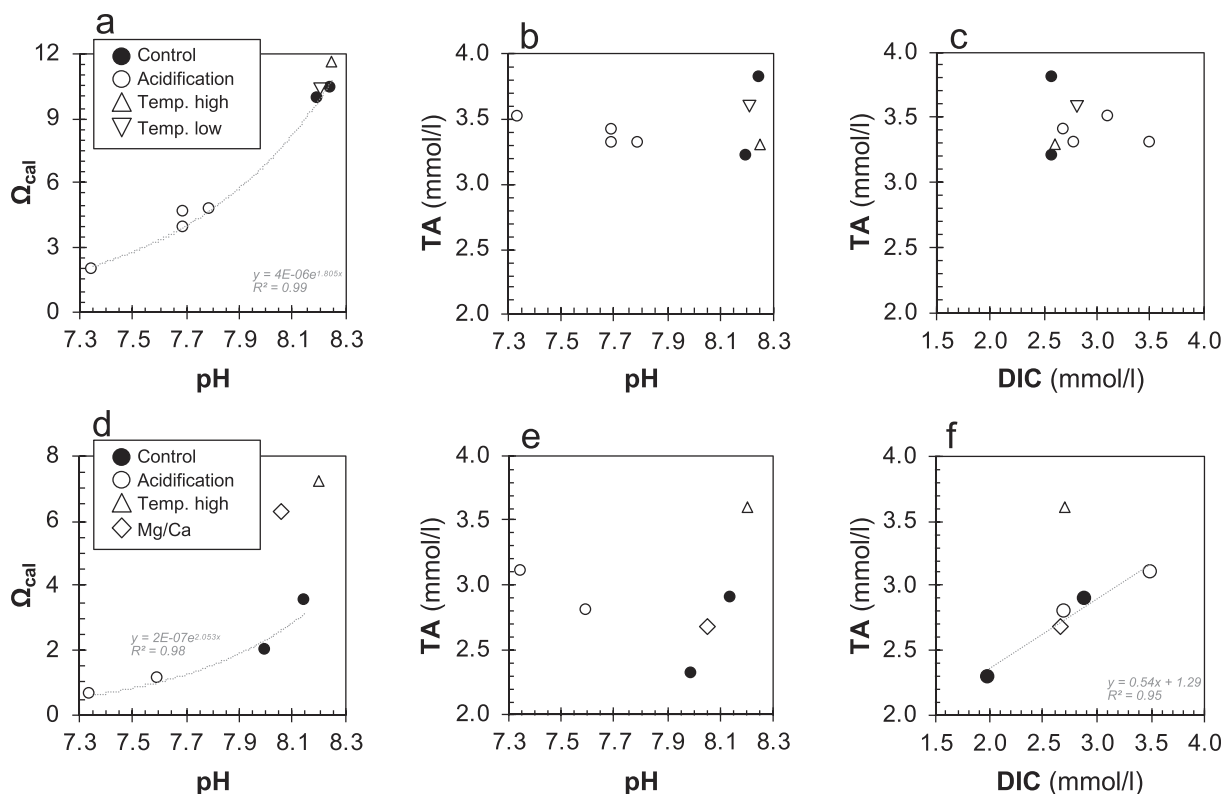
Fig. 3. Seawater carbonate chemistry in the cultures. Relationships between Ω_{cal} and pH; total alkalinity (TA) and pH, and TA and dissolved inorganic carbon (DIC) in *P. atlantica* (a–c) and *M. venosa* (d–f) aquariums.

3.2. Partitioning of elements in *Magellania venosa* with carbonate system parameters

Linear regressions describing the partitioning of Li, B, Na, Mg, Sr, and Ba into *M. venosa* calcite as a function of culture medium carbonate chemistry (pH and DIC, which as discussed above essentially also represent Ω_{cal} and TA, respectively) are presented in Fig. 4, and summarised in Table 2 (reported as $K_{D(X)} \times 10^3$ for a given element X).

For Li, the average $K_{D(Li)}$ varied between about 12.5 and 14 ($\times 10^3$), with measured lower values under acidified conditions that generally increased with pH (and/or Ω_{cal}; Fig. 4a[1]). Although we observed some scatter in the data from the moderate acidification treatment ($pH_1 = 7.6$) and its corresponding control ($pH_0 = 8.0$), the scatter was minimal for the other acidification treatment (treatment $pH_2 = 7.35$) and the control ($pH_0 = 8.0$). The average $K_{D(Li)}$ were significantly different for pH of 7.35 and 8.15 (T-test = 0.0177, df = 5, at 95% confidence level). No trend in $K_{D(Li)}$ with DIC (and/or TA) was recorded (Fig. 4a[2]).

The average $K_{D(B)}$ values varied greatly, from 320 at $pH_0 = 8.15$ and 37 at $pH_0 = 8.0$, to about 1100 at $pH_1 = 7.6$ and 200 at $pH_2 = 7.35$ (Fig. 4b). We did not observe any clear relationship with pH (and/or Ω_{cal}; Fig. 4b[1]). A slight trend towards higher $K_{D(B)}$ with increased DIC (and/or TA) may be contemplated, however it is most probable that B partitioning in each treatment

was primarily governed by other than carbonate chemistry parameters (Fig. 4b[2]).

The distribution of Mg (Fig. 4c) and Sr (Fig. 4d) followed an overall very similar behaviour. The average $K_{D(Mg)}$ varied between approximately 0.9 and 1.1 (note that the partition coefficients are reported as $K_{D(X)} \times 10^3$). We did not observe any trend with pH, but the $K_{D(Mg)}$ were generally higher for the culturing treatments of the second phase ($pH_2 = 7.35$ and $pH_0 = 8.15$; Fig. 4c[1]), where the DIC (and/or TA) was elevated (Fig. 4c[2]). $K_{D(Sr)}$ ranged between 170 and 250, and likewise increased with DIC (and/or TA; Fig. 4d[1] and d[2]).

$K_{D(Ba)}$ ranged between about 320 and 360, without any apparent systematic trend with changes in seawater carbonate chemistry (Fig. 4e). Similarly, no tendency for $K_{D(Na)}$ was found, with the average values ranging between 0.16 and 0.23 (Fig. 4f).

3.3. Changes in elemental ratios in *Magellania venosa* with temperature and culture medium chemistry

In order to carry out a detailed evaluation of the Mg/Ca temperature proxy in brachiopods we included experiments where the temperature and Mg/Ca ratio of the culture medium (Mg/Ca_{CM}) were altered. This allowed for discriminating between the effects of temperature and changes in the 'baseline' chemical composition of the CM on the measured elemental ratios in *M. venosa*. In Fig. 5 we show the Mg/Ca
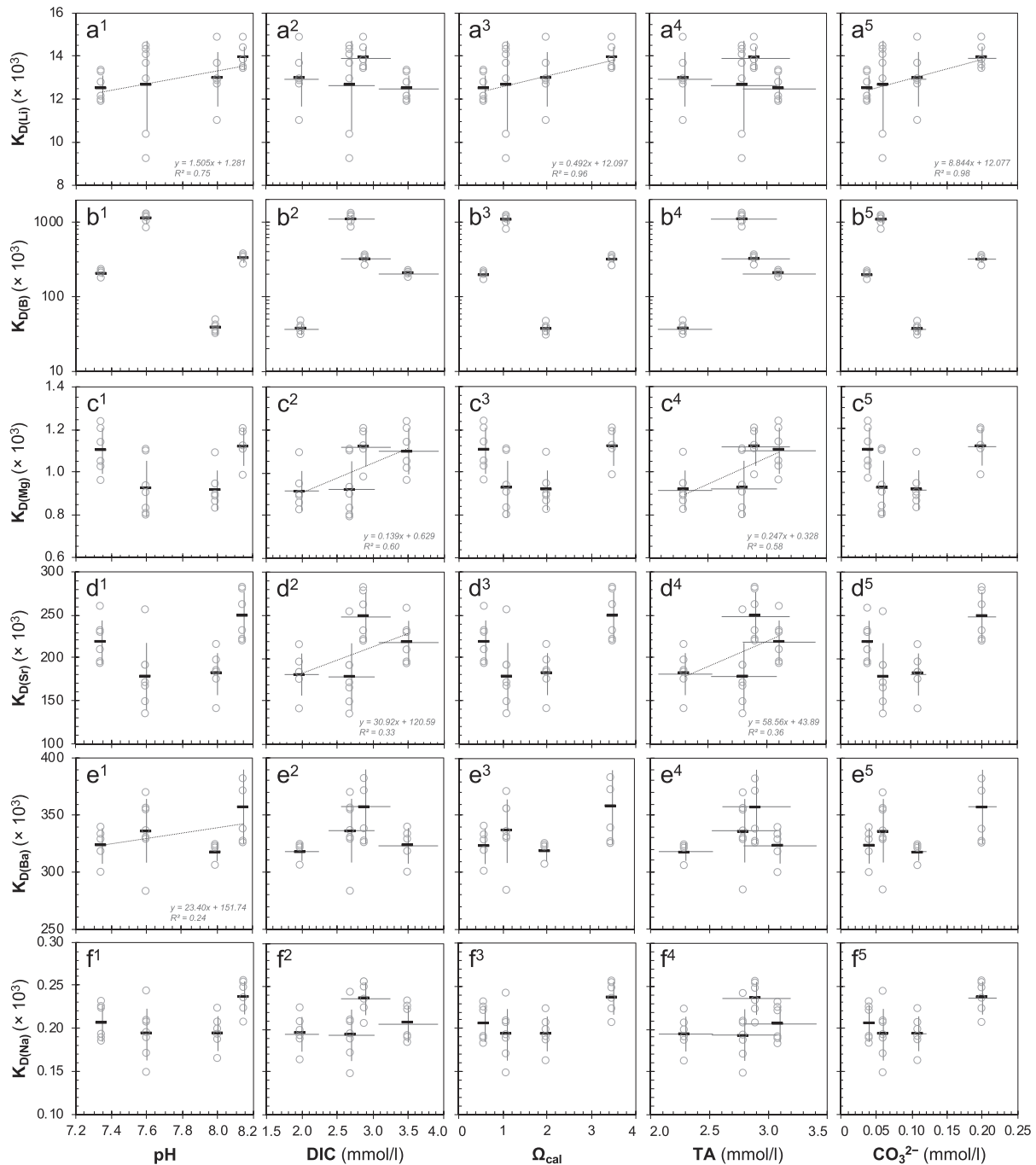
Fig. 4. Partitioning of: (a) Li; (b) B; (c) Mg; (d) Sr; (e) Ba; and (f) Na between seawater and calcite of *M. venosa* grown under varying carbonate chemistry conditions in the control and acidification experimental treatments. Partitioning coefficients $K_{D(X)}$ for each element are shown as a function of pH, DIC, Ω_{cal}, TA, and CO_3^{2-}. Grey circles show all the data points based on individual measurements in brachiopod shells (typically $n = 6$–7) and black rectangles the average values, with y-axis error bars illustrating the standard deviation (1σ) between all the data points and x-axis error bars the seawater variations in the given treatment (1σ). Because of the coupling of pH and Ω_{cal}, and DIC and TA in our cultures (see Fig. 1), analogous $K_{D(X)}$ trends are evident for pH, Ω_{cal} and CO_3^{2-}, and DIC and TA.

results, accompanied by other key elemental ratios, specifically Sr/Ca, Li/Ca and Li/Mg, which have also previously been considered as potential proxies for inferring seawater temperatures. The average Mg/Ca in the *M. venosa* calcite (Mg/Ca$_{cal}$) ranged between 5.3–6.4 mmol/mol in the con-

trol, acidification as well as the Mg/Ca treatments maintained at 10 °C. Higher Mg/Ca ratios of approximately 10.8 mmol/mol were observed in the treatment with increased temperature of CM to 16 °C (Fig. 5a). Incorporation of more Mg into the crystal lattice at higher

Table 2

Average composition of brachiopods and seawater from each treatment, and resulting mean partitioning coefficients, with SD based on variations between individual brachiopods. More detailed data including individual measurements is available in the Supplement. Note that, for convenience, $K_{D(X)}$ values are reported as $K_{D(X)} \times 10^3$, and $K_{D(B)}$ was calculated from seawater $B(OH)_4^-/HCO_3^-$.

| Aq. No.	Treatment	ID	Sample	Li/Ca µmol/mol	B/Ca µmol/mol	$B(OH)_4^-/HCO_3^-$ mmol/mol	Mg/Ca mmol/mol	Sr/Ca mmol/mol	Ba/Ca µmol/mol	Na/Ca mmol/mol
Phase 1 (P1): August 2016 − April 2017										
B3	Temp. high	T+	*M. venosa*	27.17	392.22	–	10.82	1.31	20.05	9.90
B3	Temp. high	T+	seawater	2367	57,704	2.528	5572	6.905	50.77	44,517
			K_D (×10³), n = 1	*11.48*	*–*	*155*	*1.94*	*189*	*395*	*0.22*
C1	Mg/Ca	Mg/Ca	*M. venosa*	29.51	585.57	–	5.27	1.04	13.72	9.66
C1	Mg/Ca	Mg/Ca	seawater	1569	38,567	1.046	3711	4.734	32.37	30,864
			K_D (×10³), n = 1	*18.81*	*–*	*560*	*1.42*	*221*	*424*	*0.31*
C2	Control	pH0	*M. venosa*	34.14	479.73	–	5.79	1.48	16.59	10.15
C2	Control	pH0	seawater	2641	64,994	13.075	6335	8.192	52.17	52,294
			K_D (×10³)	*12.93*	*–*	*37*	*0.91*	*181*	*318*	*0.19*
			SD, n = 6	*1.27*	*–*	*6*	*0.09*	*24*	*8*	*0.02*
C3	Acid. (pCO2)	pH1	*M. venosa*	32.52	397.32	–	5.70	1.45	17.33	10.15
C3	Acid. (pCO2)	pH1	seawater	2575	64,045	0.364	6182	8.129	51.52	52,565
			K_D (×10³)	*12.63*	*–*	*1092*	*0.92*	*178*	*336*	*0.19*
			SD, n = 7	*2.08*	*–*	*147*	*0.13*	*39*	*28*	*0.03*
Phase 2 (P2): April 2017 − July 2017										
C2	Control	pH0	*M. venosa*	39.14	415.30		7.39	1.88	16.72	12.33
C2	Control	pH0	seawater	2817	72,676	1.292	6605	7.567	46.79	52,339
			K_D (×10³)	*13.90*	*–*	*322*	*0.93*	*248*	*357*	*0.24*
			SD, n = 6	*0.54*	*–*	*33*	*0.46*	*29*	*32*	*0.02*
C2	Control	pH0	*T. dorsata*	37.80	442.19		7.05	1.82	16.21	11.94
C2	Control	pH0	seawater	2817	72,676	1.292	6605	7.567	46.79	52,339
			K_D (×10³)	*11.75*	*–*	*415*	*0.92*	*212*	*308*	*0.20*
			SD, n = 2	*0.02*	*–*	*7*	*0.05*	*19*	*21*	*0.01*
C3	Acid. (pCO2)	pH1	*M. venosa*	36.75	333.28	–	7.63	1.74	15.60	11.62
C3	Acid. (pCO2)	pH1	seawater	2945	76,602	1.652	6941	7.980	48.28	56,422
			K_D (×10³)	*12.48*	*–*	*202*	*1.10*	*218*	*323*	*0.21*
			SD, n = 6	*0.63*	*–*	*17*	*0.11*	*25*	*16*	*0.02*
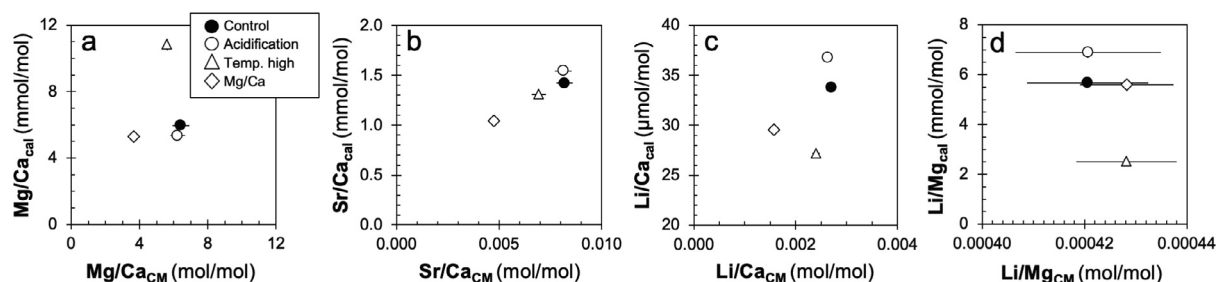
Fig. 5. Variations in: (a) Mg/Ca; (b) Sr/Ca; (c) Li/Ca; and (d) Li/Mg ratios in the brachiopod calcite and culture medium in the different culturing treatments (control, acidification, high temperature, and the Mg/Ca experiment with modified seawater chemistry).

temperatures is also visible from the EMP Mg map (Fig. 6). Higher Mg content is present in the shell part grown in the experimental treatment in contrast to the shell part grown in nature before culturing.

Opposed to the Mg/Ca trend, the Sr/Ca ratios showed a positive linear trend, with increasing Sr/Ca_{cal} from ~1.0 mmol/mol to ~1.5 mmol/mol as a function of Sr/Ca_{CM} (Fig. 5b). The Li/Ca ratios, on the other hand, possibly hint towards a weak decreasing trend with temperature, albeit with comparatively large variations between the treatments (between 27.2 and 36.8 μmol/mol) that may not be clearly linked to environmental conditions (Fig. 5c). Finally, similar to Mg/Ca, the Li/Mg composition of the shells was apparently related to the CM temperature, with decreasing Li/Mg from between 6.9 and 5.6 mmol/mol at 10 °C to 2.5 mmol/mol at 16 °C, yet with substantial variations between treatments of the same temperature as well (Fig. 5d).

3.4. Punctae (pore space) volume

To quantify the changes in the microstructure of *M. venosa* as a result of different ambient and CM conditions we report the punctae volume content (Table 3). The punctae contents were calculated for selected regions of interest in the natural specimen (Fig. 7a), and specimens from the distinct culture treatments – control ($pH_0 = 8.15$; Fig. 7b), acidification ($pH_2 = 7.35$; Fig. 7c) and high temperature (Fig. 7d). To account for changes caused by ontogenetic trends, the regions of interest were always placed in the anterior part of the shell, and scanned samples were mature individuals of similar size (Fig. 1). The internal variability was minimal, with highly comparable total punctae

Table 3
Calculated punctae volumes (%) from μCT scans of selected *M. venosa* shell areas as illustrated in Fig. 7.

M. venosa treatment	Box (Fig. 7)	Punctae volume (%)
Nature	a^1	13
	a^2	13
	a^3	14
Control		13
Acidification (pH_2)		17
Temperature (high)		24

volumes of 13–14% calculated in the different boxes of the natural sample. Similarly, the punctae volume from shells cultured under control conditions was 13%, highly comparable to the shells from nature. At acidified conditions (pH_2) the volume increased to about 17%. Most pronounced change was observed in the shell cultured under thermal stress, where the punctae volume increased to 24%, indicating that relatively more pore space was present at high temperature than under normal conditions.

4. DISCUSSION

Out of the cultured brachiopods only *M. venosa* was abundant in all the experimental treatments (*T. dorsata* was limited to the control tank) and produced discernible new shell material suitable for further investigations of the incorporation of major and trace elements into the calcite and punctae assessment, which are further discussed. We note, however, that the elemental composition of *T. dorsata* was largely within the range of the values obtained
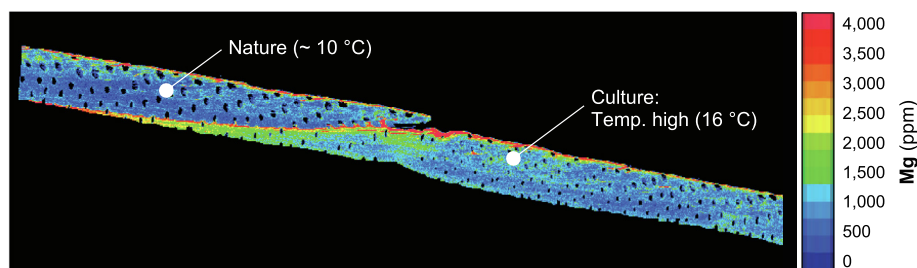

Fig. 6. Electron microprobe (EMP) image showing the Mg distribution in the anterior shell part of *M. venosa* precipitated under natural conditions (with average seawater temperatures in the habitat around ~10 °C) and under elevated temperatures during the culturing experiments (16 °C).
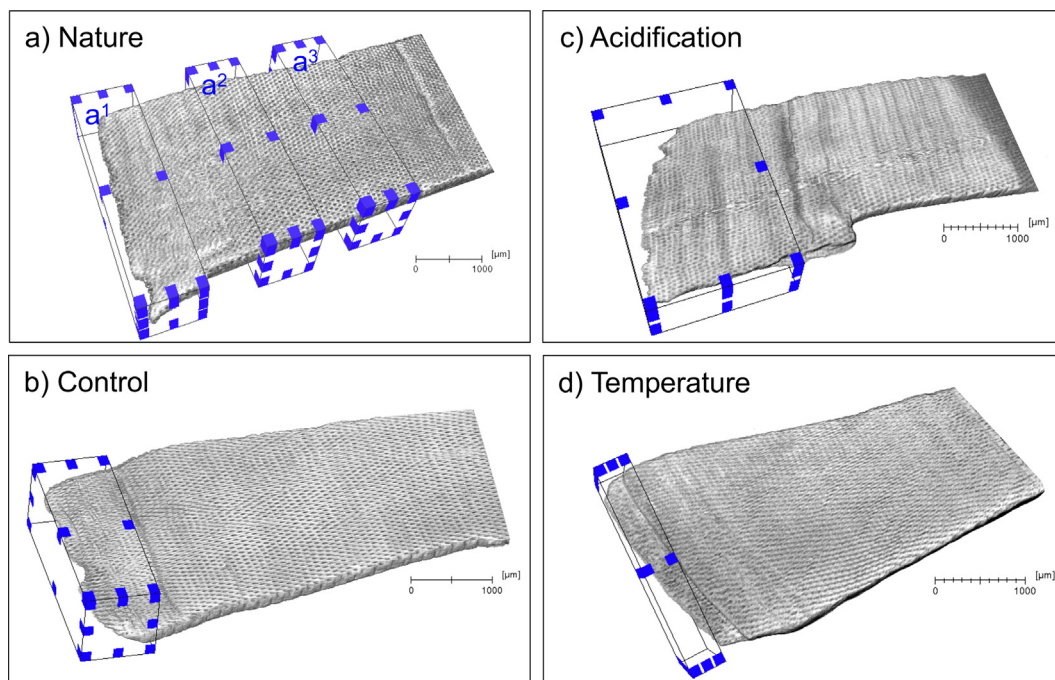
Fig. 7. μCT reconstructions of the scanned *M. venosa* shell parts from an individual grown under: (a) natural conditions in Chile; (b) control; (c) acidification (pH$_2$) and (d) high temperature treatment in the cultures. Blue boxes indicate the selected regions of interest for quantification of punctae volumes. (For interpretation of the references to colour in this figure legend, the reader is referred to the web version of this article.)

for *M. venosa* from the same control treatment (for the studied ratios; Table 2). Similarities in the elemental, as well as the boron isotope composition (Jurikova et al., in press-a) between *M. venosa* and *T. dorsata*, might therefore suggest that our findings could be potentially applicable to more than one brachiopod species, at least terebratellids with close phylogeny.

4.1. Implications for the use of elemental ratios as proxies

Over the past years B/Ca ratios of marine calcifiers (e.g. Douville et al., 2010; Jurikova et al., in press-b), and principally in foraminifera (e.g. Yu et al., 2007; Rae et al., 2011; Allen and Hönisch, 2012; Henehan et al., 2015), have gained increased attention as a proxy for past ocean carbonate system changes. However, the controls on boron incorporation still remain unclear and the proxy relationships confounding. While the boron isotopic composition of marine calcifiers is commonly controlled by pH, this is usually not apparent in B/Ca, despite that Eq. (3) predicts that the B/Ca will be a function of $[\mathrm{B(OH)_4^-/HCO_3^-}]$ in seawater which is pH dependent (Yu and Elderfield, 2007). Our experiments further support this notion, as we did not identify any relationship between the $K_{D(B)}$ values and carbonate system parameters (Fig. 4). In particular, B incorporation did not appear to be at all driven by changes in culture medium pH (and/or Ω_{cal}), contrary to the theoretical basis of the proxy and to the findings that in cultured foraminifera B/Ca have been found to strongly correlate with seawater pH (Allen and Hönisch, 2012; Henehan et al., 2015). It is possible that the lack of trend with pH

in *M. venosa* is to a certain extent caused by the physiological regulation of their calcifying fluid's pH, which appears to be maintained at only a narrow range (Jurikova et al., in press-a). An additional factor could be internal heterogeneities in B content of the calcite, originating in comparatively more complex biomineralisation mechanisms than foraminifera, for example. Similarly, based on our results, it is difficult to link the observed varying $K_{D(B)}$ values to changes in DIC and/or TA or other environmental parameters and CM conditions, and thus the dominant control on B incorporation in brachiopod species studied here still remains unsettled. Especially, questions remain on the drivers behind the broad range in partitioning of B observed in the different culturing treatments. For instance, under moderate acidification conditions, the $K_{D(B)}$ was by more than a factor of three higher than in the other aquariums, which cannot be explained in context of carbonate system chemistry or other monitored parameters in the cultures. Hence, while the boron isotope pH-proxy (δ^{11}B) appears promising for brachiopods (Lécuyer et al., 2002; Penman et al., 2013; Jurikova et al., in press-a), suggesting that the large variations in $K_{D(B)}$ are not coupled with B fractionation, the B/Ca are difficult to link to changes in seawater carbonate chemistry and further studies evaluating the B systematics are needed before B/Ca might present a meaningful proxy in brachiopods.

Although variations in Li/Ca of brachiopod shells have been principally attributed to temperature changes (Delaney et al., 1989), multiple controls on the incorporation of Li into other marine calcifiers have been identified including mineralogy, salinity, temperature and/or

carbonate system parameters (Lear et al., 2010; Marriott et al., 2004a; Vigier et al., 2015; Raddatz et al., 2013). Recent studies on foraminifera postulated a link between Li/Ca (Doss et al., 2018) or lithium isotope composition (δ^7Li) of benthic foraminifera (Roberts et al., 2018) and carbonate chemistry, in particular changes in pH and carbonate ion concentration, respectively. However, at the same time Li/Ca ratios were found to be subjected to confounding effects from temperature, which needs constraining prior to attempting any palaeo-oceanographical reconstructions, complicating the use of this ratio as a proxy (Doss et al., 2018; Marriott et al., 2004a, 2004b). While Dellinger et al. (2018) principally focused on the δ^7Li of brachiopods and molluscs, they also reported an inverse correlation between Li/Ca and δ^7Li, suggesting that a single process may determine both. The authors proposed that this could result from the lowering of the Mg/Ca ratio of the calcifying fluid during which a combined removal of Mg and Li may occur. This however appears unlikely, at least for *M. venosa*, as based on our culture-based dataset no link between Mg and Li incorporation was observed, and moreover, different processes seem to influence each element. At a first sight, our results appear to indicate that brachiopods incorporate relatively more Li with increasing pH and/or Ω_{cal} of the CM (Fig. 4a). Superimposed over this is the highly variable Li/Ca_{cal} that seems to be also partially affected by temperature, even though in general it remains difficult to link Li/Ca_{cal} variations to specific environmental conditions or the Li/Ca_{CM} (Fig. 5a). Such diverse trends are also in line with the already mentioned varied controls postulated in the literature. Accounting for changes in the carbonate chemistry in the high temperature and Mg/Ca culturing tanks (as detailed in Section 3.1), we find that Li/Ca ratio appears to be closely dependent on the Ω_{cal} of the culture medium (Fig. 8a). However, when the contribution from Li/Ca_{CM} is considered and we look at the $K_{D(Li)}$ it becomes clear that the incorporation of Li into the shell is in addition strongly affected by changes in the CM chemistry and temperature (Fig. 8b). This example illustrates very well the problems associated with the calibration and application of simple elemental ratios as proxies. In the absence of information on the chemical composition of CM, the strong linear fit ($R^2 = 0.96$) between Li/Ca_{cal} and Ω_{cal} could be interpreted as evidence supporting the use use of Li/Ca_{cal} ratios as a proxy for Ω_{cal}, which as discussed

above is clearly misleading (Fig. 8a). One could even further argue that neither temperature (in the range of ΔT of 6 °C) nor growth-dependent kinetic effects (taking into account that under increased temperatures *M. venosa* shell growth was reduced by approximately ½, see Section 3.1) or the seawater chemical composition (addition of $CaCl_2$ in the Mg/Ca treatment) seem to be of significant influence to Li/Ca_{cal} in *M. venosa*, based on the close correlation. However, Fig. 8b clearly shows that exactly the opposite is true, with all these parameters (i.e. temperature, growth-effects as well as seawater chemistry) apparently strongly confounding any potential response of Li/Ca_{cal} to carbonate system parameters. This might explain the contrasting results from literature, and calls for a more comprehensive approach to calibrating elemental proxies, assessing multiple factors at the same time. Until then, straightforward use of Li/Ca as proxy in brachiopods, but most likely in other marine calcifiers as well, should be considered problematic and treated with caution.

Both Mg/Ca and Sr/Ca present rather well studied ratios in marine calcifiers that have been traditionally linked to seawater temperatures (Beck et al., 1992; Nürnberg et al., 1996; Mitsuguchi et al., 1996). A growing number of studies, however, suggest various factors as being responsible for influencing the incorporation of these elements into marine biogenic calcium carbonate including seawater chemistry, carbonate chemistry, growth and/or physiological effects (e.g. Russell et al., 2004; Raitzsch et al., 2010; Tanaka et al., 2019). Similarly, Mg/Ca in brachiopods has been found to generally record seawater temperature (e.g. Pérez-Huerta et al., 2008; Powell et al., 2009; Butler et al., 2015), although as most brachiopods precipitate low-Mg calcite, the use of the ratio as a proxy has been questioned by studies attributing Mg incorporation to physiological controls rather than environmental conditions (Buening and Carlson, 1992; England et al., 2006). Certainly, across a broad spectrum of brachiopod taxa or other calcifiers the most prominent control on the incorporation of Mg or Sr (as well as other elements) seems to be phylogeny (Ullmann et al., 2017). However, it appears that the origin of intraspecific and even intra shell variations still requires further evaluation (Rollion-Bard et al., 2019). Our culturing results indicate a strong co-variance between Mg/Ca and Sr/Ca in *M. venosa* (Fig. 4c and d), and could potentially imply that the incorporation of both may be controlled by a common mechanism. Co-variance of Sr and Mg in analogous modern and ancient marine calcite has been previously reported by Carpenter and Lohmann (1992), and in brachiopods principally ascribed to rhynchonellids only (Ullmann et al., 2017). The origin of the covariance across a range of calcites has been proposed to bear a link to the secular variation in ocean Sr, Mg and Ca concentrations (Carpenter and Lohmann, 1992). It may be expected that secular variations in chemical composition of the ocean beyond residence time of the given element drive the 'baseline' composition of a calcite, however, this still does not satisfactorily explain changes in Sr/Mg composition of a shell over, for instance, an individual's lifetime, or under different environmental conditions.
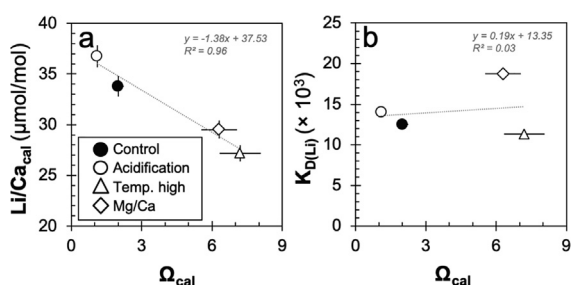

Fig. 8. Variations in (a) Li/Ca and (b) $K_{D(Li)}$ of *M. venosa* in relationship to the changes in culture medium Ω_{cal} in different treatments.

We found, noticeably, that the Mg/Ca and Sr/Ca ratios in *M. venosa* individuals were clearly offset between the two culturing phases – less Mg and Sr was incorporated during the first culturing phase P1 in contrast to the later phase P2 (Fig. 4c and d). The principal difference between the culturing phases was the TA and DIC content, both were higher during P2 than P1, indicating that either TA and/or DIC could control the incorporation of Mg and Sr into *M. venosa*. TA summarises the carbonate system parameters including the two main dissolved ions – HCO_3^- and CO_3^{2-}, which are also the major proportions of DIC. Hence the sum of the two ions may be considered as a principal controlling factor. In the following, we opt for considering DIC as a more likely candidate since TA is a conceptual parameter for describing the carbonate system, rather than a condition relevant for an organism's biological regulation. Recent experiments on foraminifera point towards DIC as being an instrumental parameter in controlling the Sr incorporation (Keul et al., 2017). Similarly, Keul et al. (2017) found highest Sr content in tests cultured under increased pCO_2 and thus DIC, suggesting that the changes observed in our brachiopods might also be caused by DIC. One of the possible mechanisms driving this relationship could be the regulation of Ω_{cal} in the calcifying fluid. To maintain a stable Ω_{cal} of the calcifying fluid, a decreased influx of Ca ions regulated by decrease in Ca-ATPase activity is necessary under concurrent enhanced DIC influx, which would affect the Sr/Ca_{cal} and with it the $K_{D(Sr)}$. This could explain the observed Sr partitioning trends in our cultures, and is further explored in Section 4.2. However, it is unclear why Mg would be affected by the same transport mechanisms, since in contrast to Sr it is not a physiologically inert divalent cation. For instance, in coccolithophores an increased $K_{D(Sr)}$ and $K_{D(Mg)}$ were found under elevated pCO_2, however numerous lines of evidence point towards distinct pathways for Mg in contrast to Sr and Ca to the calcification site (Müller et al., 2014). Thus, currently, despite the clear trend in our data that may indicate a common mechanism for partitioning of Mg and Sr into *M. venosa* shells, it is inconclusive if a single common pathway for Mg and Sr exists in brachiopods, or whether this is a coincidence. Mg plays a vital role in energy demanding processes as ATP activator in numerous enzymatic reactions (Nadler et al., 2001), and it is possible that under higher pCO_2 stress and thus DIC conditions, an increased input of Mg would be required for optimal functioning.

In addition to the experiments with modified carbonate system chemistry, *M. venosa* were also cultured under elevated temperatures and adjusted Mg/Ca_{CM} ratio of culture medium, enabling us to further evaluate the Mg/Ca and other temperature proxies. Our results indicate that a significant change in Mg/Ca_{cal} ratio occurred at higher ambient temperatures, and was not influenced by changes in Mg/Ca_{CM} (Fig. 5a). Furthermore, *M. venosa* grown under increased temperatures built calcite systematically enriched in Mg throughout the whole new shell (Fig. 6), which could potentially indicate a temperature dependency. However, the confounding effects of growth and specific shell features, as well as DIC have to be taken into account. Similar to

bivalves for example, we observed the shell growth lines to be more enriched in Mg than the growth increments, a likely result of enhanced Mg incorporation by organic matter (Tanaka et al., 2019). Moreover, in contrast to the other *M. venosa* culturing treatments, new shell growth of all individuals cultured under higher temperatures was reduced in length. This makes it difficult to isolate the growth-specific influence on Mg partitioning, which appears to be at least partially present in *M. venosa* and other brachiopods (e.g. England et al., 2006; Cusack et al., 2008; Jurikova et al., in press-a). The homogenous enrichment in Mg in the shell increment precipitated under increased temperature could certainly lend support for a positive dependency on temperature. However, an increased influence from kinetic effects due to decreased precipitation rates on the Mg/Ca should also be assumed. Decreased precipitation rates lead to increased Mg concentrations in calcite (Gabitov et al., 2014; Ullmann and Pogge von Strandmann, 2017), and hence our observed Mg/Ca trends in *M. venosa* could be solely explained in terms of changing growth rates. Discriminating between growth vs. temperature effects in nature poses a challenge, as size and temperature are intimately linked in numerous marine calcifiers and a broad range of organisms in general following fundamental ecological and metabolic rules, and should be considered in studies attempting to calibrate geochemical temperature proxies. We propose a possible solution for constraining growth effects by structural analyses (specifically, by quantifying the punctae volume in the shell), which is further discussed in Section 4.3.

4.2. A biomineralisation model perspective on Sr partitioning

Over recent years, the number of studies assessing the geochemical composition of brachiopod shells has been on the rise. However, a mathematical model for explaining elemental trends is still lacking. In order to further explore the observed X/Ca variations and to put our data within a quantitative framework, we devised the first biomineralisation model for brachiopods. Our simple model is principally based on Sr^{2+} incorporation, and is intended for examining the observed Sr/Ca response to changes in carbonate chemistry, more specifically DIC (Fig. 4). Similar to Sr/Ca, we also found Mg/Ca to vary with DIC, but given that Mg could be considered as a physiologically relevant element and low-Mg calcite-building brachiopods probably actively discriminate against Mg, its incorporation mechanisms are likely less straightforward than for Sr and hence was not considered for the model. Potentially, the model could also be relevant for other large physiologically-inert divalent cations such Ba^{2+} that may follow similar incorporation pathways as Sr^{2+}, or adapted for monovalent cations such as e.g. Li^+ or Na^+, although the incorporation of these is less straightforward as one-to-one substitution with Ca^{2+} cannot be considered (e.g. Füger et al., 2019).

Our model is based on previously proposed concepts for foraminifera (Erez, 2003; Nehrke et al., 2013; Keul et al., 2017), corals (Cohen and McConnaughey, 2003; McCulloch et al., 2012), coccolithophores (Langer et al., 2006) and gastropods (Langer et al., 2018), and adapted

to brachiopods based on the current understanding of their calcification mechanisms (Schmahl et al., 2004; Jurikova et al., in press-a). Given the comparatively limited knowledge on the physicochemical processes involved in brachiopod biomineralisation than in the other calcifiers, we note that rather than a definite framework, our model should be considered as exploratory, and awaits further validation and potential refining in future research.

In the model, we assume that calcification occurs in a semi-closed calcification space between the epithelial mantle and the shell (Figs. 9 and 10). This space is of several μm or sub-μm dimensions and filled with a fluid – calcifying fluid (hereinafter CF) – where the precipitation of new calcite crystals takes places, separated from the ambient seawater by a membrane. The partitioning of elements between seawater and calcite is defined by the partition coefficients ($K_{D(Sr)}$ for Sr) as given in Eq. (1). Since information on the chemical composition of the CF is not available, we assume that it is largely similar to that of seawater, precisely the culture medium. We consider that the transport of ions through the membrane occurs via two main processes – trans-membrane transport (TMT) and passive transport (PT).

The active transport of ions through the membrane termed TMT occurs via ion-transporting channels and is strongly biologically controlled. Selective TMT of ions in marine calcifiers can be controlled via specific enzymes, for instance Ca^{2+} transport through the epithelial tissue is known to be regulated by the enzyme Ca-ATPase (e.g. Cohen and McConnaughey, 2003). Simultaneously, it allows for maintaining charge balance by the Ca-ATPase-bound export of two H^+ for each Ca^{2+}. This process may also be reversible. Biological regulation of Mg is, for example, thought to be controlled by Mg-ATPase, which exports Mg^{2+} cations while importing H^+ ions (Zeebe and Sanyal, 2002).

Unlike TMT, the PT ensues through epithelial mantle and does not discriminate against selected ions, and thus does not require charge balancing. The PT serves for replenishing of the CF, and is thought to function via regulated diffusion through the epithelium enabling a replacement of 'old' CF with 'new' seawater. Through PT,
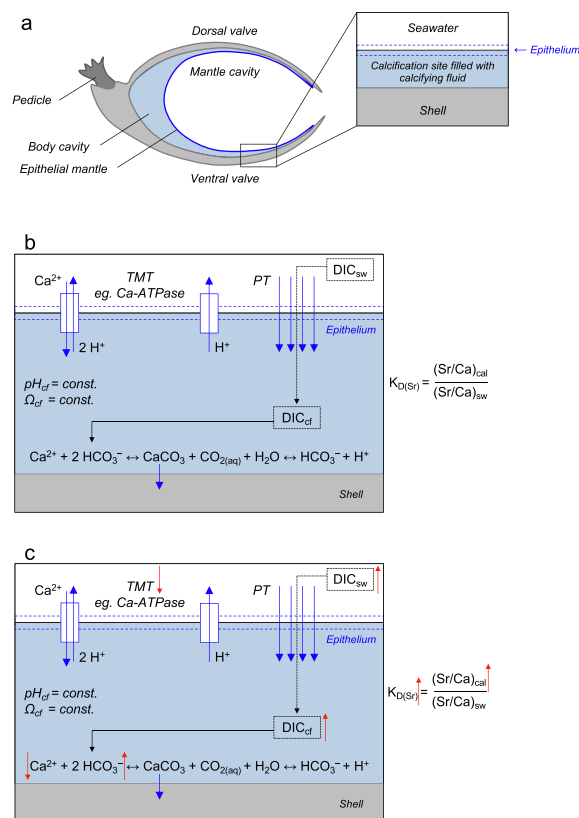

Fig. 10. Schematic representation of the brachiopod model: (a) a simplified diagram of *M. venosa* shell and the boxes in the model; (b) the considered transport mechanisms – passive (PT) and trans-membrane transport (TMT) delivering ions from the medium (culture medium or seawater) through the epithelium to the calcification site at normal ambient conditions; (c) changing relative importance of the transport mechanisms and the internal chemistry under increased DIC conditions in the medium, indicated by red arrows. (For interpretation of the references to colour in this figure legend, the reader is referred to the web version of this article.)

unfractionated elemental ratios are transported to the site of calcification from seawater, and carbon species are
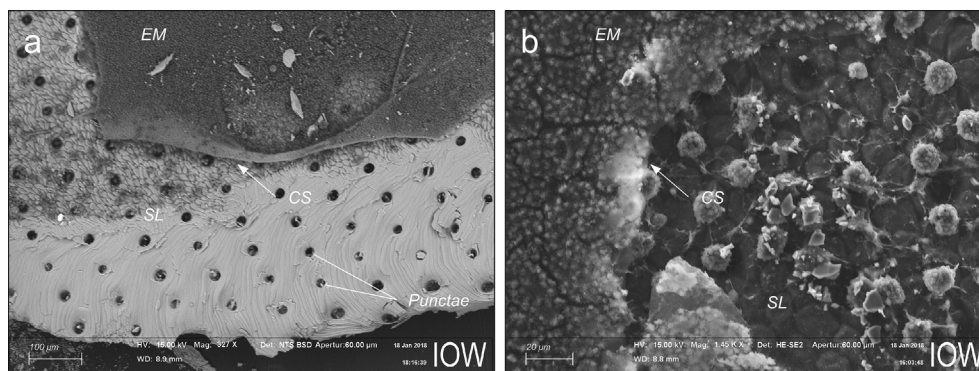

Fig. 9. Scanning electron microscope (SEM) images of a *M. venosa* shell with preserved organic tissues showing the calcification site between the innermost secondary shell layer and the epithelial mantle; (a) a large part of the mantle extending over the inner surface is visible; (b) a zoom in perspective with a detailed view of the mantle and fibres forming the inner secondary layer. EM – epithelial mantle; SL – secondary layer; CS – calcification site, located between the innermost secondary layer and the epithelial mantle.

imported that provide the calcification substrate. In contrast to other calcifiers such as foraminifera or corals, given the comparatively low pH_{CF} ($\sim$7.8) this is most likely HCO_3^- instead of CO_3^{2-} in *M. venosa*, which is the dominant DIC species in seawater at the pH and hence the calcification substrate. The following equations describe the calcification reaction:

$$Ca^{2+} + HCO_3^- \leftrightarrow CaCO_3 + H^+ \tag{7}$$

$$Ca^{2+} + 2HCO_3^- \leftrightarrow CaCO_3 + CO_2 + H_2O \tag{8}$$
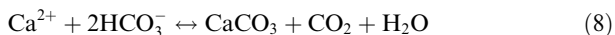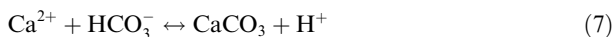
As implied by Eq. (7), the reaction releases H^+ into the CF, which cannot be compensated by the TMT as Ca^{2+} import and H^+ export via this pathway are intimately linked. To maintain a homeostatic control additional H^+ channels regulated by a voltage gradient between the CF and the seawater (Taylor et al., 2011) or other ATP-driven H^+ pumps or exchanges must also exist. In such a case, the export or import of protons could be initialised by a voltage resulting from a charge surplus or deficit in the CF with respect to ambient seawater or an ATP-driven enzyme.

Generally, TMT is characterised by differences in selectivity for different elements (Langer et al., 2006). For instance, a typical Ca^{2+} channel strongly discriminates against Mg^{2+}, which surface charge density is different to that of Ca^{2+} or Sr^{2+} (Allen and Sanders, 1994). However, given the similarity of Ca^{2+} and Sr^{2+} ions, it is likely that in addition to PT, Sr^{2+} is also co-transported to the CF via Ca^{2+} channels. This can also be supported by the much lower measured $K_{D(Mg)}$ than $K_{D(Sr)}$ (on the order of two magnitudes; Fig. 4, Table 2). We assume that the Sr/Ca transported via TMT fractionates against Sr (at least to some extent, even if not as strong as against Mg), and does not equal to seawater/CM and hence PT (and that the Ca^{2+} activity changes with DIC, as discussed onwards). Following McCulloch et al. (2012) we assume that DIC is transported to the calcification site via PT. Hence, any changes in the DIC of ambient seawater (or culture medium) are expected to result in changes of the DIC in the calcifying fluid and therefore the internal carbonate chemistry. While thus far no information on brachiopods is available, recent studies on corals for example indicate that DIC (in addition to pH) may be elevated at their site of calcification (Sevilgen et al., 2019; Guo, 2019); in fact, an active accumulation of carbon species in the CF could explain the observed higher than seawater pH_{CF}. Considering that *M. venosa* calcifies at pH_{CF} close to seawater pH (Jurikova et al., in press-a), we deem it at present unlikely that they also up-regulate DIC, but note that this still poses an open question for future research. Following Jurikova et al. (in press-a), based on $\delta^{11}B$ evidence and *in vivo* microelectrode measurements in *M. venosa* we assume an almost constant calcifying fluid pH of $\sim$7.8, which is not affected by changes in ambient seawater/culture medium pH. The strong biological control over the calcifying fluid pH is necessary for maintaining constant calcification rates, which in turn probably also sustains constant Ω_{cal} in the CF. This is supported by studies reporting unaffected brachiopod survival and shell building under acidification and thermodynamically unfa-

vourable conditions in several brachiopod species including *M. venosa* (Baumgarten et al., 2013; Cross et al., 2015, 2018; Ye et al., 2019; Jurikova et al., in press-a).

To facilitate the precipitation of new calcite we assume that the CF is supersaturated with respect to calcite ($\Omega_{cal} > 1$). A supersaturated state of the CF has been reported for cold-water corals, for instance, with $\Omega_{cal} \sim 8.5$–13 achieved by regulation of internal pH (McCulloch et al., 2012; DeCarlo et al., 2017). To determine the saturation state in the CF of benthic foraminifera, Keul et al. (2017) proposed a model that takes into account the differences in the activity of Ca^{2+} in seawater and CF. They assumed an activity coefficient for seawater $\gamma_{sw} = 0.2$, granting biological regulation an activity coefficient for CF $\gamma_{CF} = 0.2$ to 1. Further, they considered a pH of 9 in the CF, and based on a linear correlation between experimentally determined $K_{D(Sr)}$ and seawater DIC proposed a supersaturated state in the CF in the range of $\Omega_{cal} \sim 5.4$–26.9. Oriented on the results of McCulloch et al. (2012) and the other studies, we assume a constant supersaturation $\Omega_{cal} \approx 10$ (hereinafter Ω_{CF}) in the CF of *M. venosa*. This value is also supported through the adaptation of the Keul et al. (2017) approach to our data and model. Considering our experimental conditions and the expected range in the activity coefficients of Ca ions in the CF, a supersaturation of $\Omega_{CF} \approx 10$ can be derived using a Ca^{2+} activity coefficient $\gamma_{CF} \approx 0.6$ (Appendix A). While this value seems to presents a reasonable estimate from our point of view in the absence of any data on brachiopods, ultimately the Ω_{cal} in CF will need to be corroborated by empirical data, for instance through further characterisation of the CF carbonate chemistry with the microelectrode technique.

Due to PT through the epithelial tissue (McCulloch et al., 2012; Nehrke et al., 2013) it is expected that any changes in the carbonate chemistry of ambient seawater (i.e. DIC or TA) also affect the CF in *M. venosa*, yet the pH remains almost constant through homeostasis ($pH_{CF} \approx 7.8 \approx$ constant). The influence from seawater/culture medium modifies the HCO_3^- concentration in CF, but similarly supersaturation remains constant ($\Omega_{CF} \approx 10 \approx$ constant). In order to keep the Ω_{CF} constant an organism needs to regulate the Ca concentration, which however would not affect the distribution of other elements. Our model thus predicts that ambient changes in the seawater/culture medium carbonate chemistry are compensated in the calcifying fluid by an active adjustment of Ca concentration in order to favour constant calcification. This could be achieved via a regulated Ca ion influx through the membrane to the calcifying fluid using known Ca-ATPase (Marshall, 1996) and transcellular Ca ion channels (Zoccola et al., 1999). Alternatively, an active efflux may be possible, but appears less probable, as the achieved saturation state through the PT is lower than that required for homeostasis, demanding a constant active Ca^{2+} influx. Since this process does not affect the other passively transported elements, the model predicts that the partitioning of other elements and specifically $K_{D(Sr)}$ will vary with changing carbonate chemistry of the medium, precisely as a function of DIC (Fig. 10). Undoubtedly, this is only applicable

to physiologically inert elements (such as Sr for instance) and also requires an assumption that an additional transport mechanism does not actively regulate their transport. This could be supported by the fact that our brachiopod $K_{D(Sr)}$ are broadly within the range of those expected for inorganic calcite (e.g. Tang et al., 2008).

In order to calculate the Ca concentration in the CF, the full carbonate system needs to be constrained. Using the given pH_{CF} and Ω_{CF} values this leaves one unknown carbonate parameter, which can be calculated from the observed $K_{D(Sr)}$ dependency on DIC, assuming that $DIC_{CF} \approx DIC_{sw/CM}$ as previously stated. Eq. (6) can therefore be rewritten as:

$$[Ca^{2+}]_{CF} = \frac{\Omega_{CF} \times K_{sp}^*}{[CO_3^{2-}]_{CF}} \qquad (9)$$

The empirical formulas and equilibrium constants were calculated following Zeebe and Wolf-Gladrow (2001). First and second dissociation constants were based on Roy et al. (1993) for artificial seawater. Henry coefficients were calculated following Weiss (1974) as recommended in Zeebe and Wolf-Gladrow (2001). The stoichiometric solubility product of calcite K_{sp}^* (specifically, crystalline calcium carbonate CCC) was calculated using the empirical formula according to Mucci (1983) from *in situ* conditions (T = 10 °C and Sal = 30, Table 1).

The calculated $[CO_3^{2-}]_{CF}$ concentration allows for deriving the $[Ca^{2+}]_{CF}$. By influencing the $[CO_3^{2-}]_{CF}$ concentration through a correlated variable we can therefore model the distribution coefficients for an element X. Taking DIC as the influencing parameter on $K_{D(Sr)}$ the carbonate system can be constrained following Zeebe and Wolf-Gladrow (2001) from:

$$[H^+] = 10^{-pH} \qquad (10)$$

$$[CO_{2(aq)}] = \frac{DIC}{(1 + \frac{K_1^*}{[H^+]} + \frac{K_1^* \times K_2^*}{[H^+]^2})} \qquad (11)$$

$$[HCO_3^-] = \frac{DIC}{(1 + \frac{[H^+]}{K_1^*} + \frac{K_2^*}{[H^+]})} \qquad (12)$$

$$[CO_3^{2-}] = \frac{DIC}{(1 + \frac{[H^+]}{K_2^*} + \frac{[H^+]^2}{K_1^* \times K_2^*})} \qquad (13)$$

To calculate the Ca^{2+} concentration directly from DIC, Eq. (13) is substituted into Eq. (9) obtaining the $[Ca^{2+}]_{CF}$, which at a constant pH_{CF} solely depends on DIC (at constant temperature, salinity and pressure).

$$[Ca^{2+}] = \frac{K_{sp}^* \times \Omega_{CF} \times (1 + \frac{[H^+]}{K_2^*} + \frac{[H^+]^2}{K_1^* \times K_2^*})}{DIC} \qquad (14)$$

The constants calculated from the empirical equations (as previously mentioned) provide the equilibrium $[Ca^{2+}]$. To express the changes in $K_{D(Sr)}$ directly from DIC, Eq. (14) is substituted into Eq. (1) giving the final formulation:

$$K_{D(X)} = \frac{\frac{[X]_{cal} \times DIC}{\Omega_{CF} \times K_{sp}^* \times (1 + \frac{[H^+]}{K_2^*} + \frac{[H^+]^2}{K_1^* \times K_2^*})}}{\left(\frac{[X]}{[Ca^{2+}]}\right)_{sw}}$$

$$= \frac{[X]_{cal} \times DIC \times [X]_{sw}}{[Ca^{2+}]_{sw} \times \Omega_{CF} \times K_{sp}^* \times (1 + \frac{[H^+]}{K_2^*} + \frac{[H^+]^2}{K_1^* \times K_2^*})} \qquad (15)$$

A comparison between the measured and modelled $K_{D(Sr)}$ as a function of DIC is shown in Fig. 11. The presented model predicts systematic increase in $K_{D(Sr)}$ with increasing ambient DIC and closely reproduces the trends observed in our culturing experiments (Fig. 11a). We note that by taking a $\Omega_{CF} \approx 1$ instead of the used value of 10 the predicted absolute $K_{D(Sr)}$ would increase by a factor of 10 (since with decreasing Ω_{CF} also $[Ca^{2+}]_{CF}$ decreases, but the $K_{D(X)}$ increases as prescribed by Eq. (1)), but the slope would remain unaffected. Similarly, any changes in DIC_{CF} would result in a linear response of the model, with increase or decrease in DIC proportionally affecting the $K_{D(Sr)}$ (i.e. an increase in DIC by 50% would increase the $K_{D(Sr)}$ by 50%).
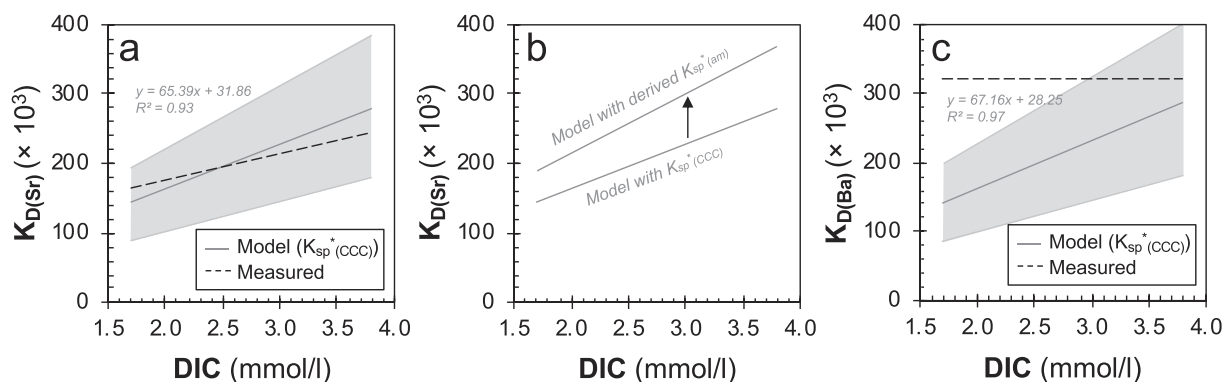

Fig. 11. Model results: (a) measured (black dashed line) and modelled (grey solid line) partitioning of Sr ($K_{D(Sr)}$) for *M. venosa* as a function of DIC content. The equation in the chart is the modelled slope and the grey bars mark the propagated slope uncertainty derived from Gaussian equation (Appendix B). This model scenario is based on a stoichiometric solubility product K_{sp}^* for crystalline calcium carbonate ($K_{sp}^*{}_{(CCC)} = 3.60 \times 10^{-7}$ mol²/l²) calculated following Zeebe and Wolf-Gladrow (2001). (b) An alternative model scenario considering biologically-mediated formation of ACC through the use of a K_{sp}^* derived from the activity model ($K_{sp}^*{}_{(am)} = 2.75 \times 10^{-7}$ mol²/l²). (c) Comparison between modelled and measured partitioning of Ba ($K_{D(Ba)}$).

The positive dependency of $K_{D(Sr)}$ on DIC can be explained in the context of biomineralisation by the substitution of Sr^{2+} for Ca^{2+} ions in the crystal lattice (Finch and Allison, 2007). In order to maintain calcification constant (and pH_{CF} and Ω_{CF}) under elevated DIC, decreasing active import of Ca^{2+} ions to the CF via TMT is necessary, leaving the reservoir relatively enriched in Sr^{2+}, thereby increasing the probability of Sr incorporation into the shell calcite (Fig. 10). As the DIC in the CF increases under increasing DIC in seawater via PT, the Ω_{CF} would also have to increase. To keep it constant, the organism would reduce the Ca^{2+} import through TMT, meaning that the relative importance of transport mechanisms would also vary as a function of DIC, with increasing relative share of PT in the total import to CF as TMT decreases. Since PT is not assumed to fractionate, at least not to physiologically inert elements, under these conditions, the composition of the CF and hence the shell approximates to that of seawater, as reflected in the increasing $K_{D(Sr)}$ trend with DIC.

Finally, we note that while our model seems to explain the observed $K_{D(Sr)}$ values, it remains, undoubtedly, a mathematical simplification of physiologically complex processes that are difficult to formulate into a modelling framework. We consider the formation of the calcite according to thermodynamic principles, which, however, cannot account for biological intervention during the crystal formation. Furthermore, the presented model assumes the formation of crystalline calcite directly out of the calcifying fluid, without an intermediate precursor step. However, it appears to be now largely accepted that calcifying organisms first secrete carbonate in the form of amorphous calcium carbonate (ACC), which is eventually reordered into a crystalline phase (e.g. Addadi et al., 2003; Politi et al., 2008; Mass et al., 2017). ACC is known to be a transient precursor in a wide range of marine calcifiers (e.g. corals, molluscs, or sea urchins) including brachiopods. It is assumed that its reordering into a crystalline phase occurs via solid state transformation upon which the chemical composition of the ACC precursor is transferred (e.g. Griesshaber et al., 2009). The reordering could, however, be potentially associated with elemental or isotopic fractionations that are challenging to constrain in a simple model. In the model, any biological influence on the reordering of ACC may be principally expressed through the stoichiometric solubility product K_{sp}^*. Our applied K_{sp}^* was calculated following Zeebe and Wolf-Gladrow (2001) and represents the value for a crystalline calcium carbonate (CCC) – hereinafter $K_{sp}^*{}_{(CCC)}$. A precursor step involving ACC formation could be potentially accounted for by assuming a K_{sp}^* for inorganic ACC – $K_{sp(ACC)}^*$ (Brečević and Nielsen, 1989). However, neither of these K_{sp}^* values takes into account the potential biological influence on calcification, and altogether K_{sp}^* values for biologically-mediated carbonates whether ACC or CCC appear to be at present poorly constrained in the literature. In an attempt to constrain biological influences and ACC reordering through a more appropriate choice of K_{sp}^*, we derive a new value from the activity model (Appendix A), hereinafter $K_{sp}^*{}_{(am)}$. The $K_{sp}^*{}_{(am)}$ can be obtained by rearranging Eq. (A4) after K_{sp}^*, and applying our previously used assumptions on activity coefficients ($\gamma_{sw} = 0.2$ and $\gamma_{CF} = 0.6$ after Keul et al., 2017; Appendix A), carbonate chemistry ($\Omega_{CF} \approx 10$, and $DIC_{sw/CM} \approx DIC_{CF}$), and using the measured average $K_{D(Sr)}$ and $[Ca^{2+}]_{sw/CM}$. This results in a mean value of $K_{sp}^*{}_{(am)} = 2.75 \times 10^{-7}$ (mol^2/l^2), which is smaller than that for inorganic CCC ($K_{sp}^*{}_{(CCC)} = 3.60 \times 10^{-7}$) or ACC ($K_{sp}^*{}_{(ACC)} = 5.42 \times 10^{-7}$). This is potentially counter-intuitive as it states that the thermodynamic stability of the $K_{sp}^*{}_{(am)}$ product over the solution would be lower than in the case of CCC. Conversely, it could explain the need for biologically-driven stabilisation of ACC. Brachiopods are known to exert strong biological control over the formation and shape of their shell fibres, which through an ACC precursor step may be achieved by and an organic template (e.g. Veis, 2003). In particular, in the absence of Mg as an alternative stabilisation mechanism, the need for biological intervention could compensate for the low $K_{sp}^*{}_{(am)}$ values. Moreover, as given in Equation (15), a decrease in K_{sp}^* would result in increased partitioning coefficients $K_{D(X)}$, predicting higher elemental concentrations in ACC than in the crystalline phase. Assuming that the elemental composition of the primary layer in brachiopods reflects or is close to that of the ACCs, as postulated from relatively lower $\delta^{18}O$ and higher elemental content (Rollion-Bard et al., 2019), it should be possible to compare the derived K_{sp}^*-dependent increase in $K_{D(X)}$ with empirical observations from this layer. Accounting for ACCs via the $K_{sp}^*{}_{(am)}$, our model predicts a roughly ~25% increase in Sr partitioning (Fig. 11b), which is also in a close agreement with the empirical evidence from Rollion-Bard et al. (2019) that situates the Sr enrichment in the primary layer relative to the secondary layer at a similar percentage range.

Finally, we also briefly test the model for Ba (Fig. 11c). As expected, given the lack of trend between $K_{D(Ba)}$ and carbonate system parameters, the measured and modelled trends differ, although the $K_{D(Ba)}$ are broadly within the range of the predicted values. We suspect that this is largely due to the fact that Ba concentration in both the calcite and culture medium is on the order of two magnitudes lower than Sr (Table 2), making it comparatively less relevant as a substituting cation in the lattice, at least within the range of experimental conditions considered in this study.

4.3. Towards punctae volume as a new quantitative proxy

In addition to geochemical signatures, changes in shell microstructures have been regarded as valuable proxies for the reconstruction of past environmental conditions (Garbelli et al., 2017; Ye et al., 2018, 2019; Glock et al., 2018). While foraminifers' pore space density has proven to be a useful indicator for inferring the dissolved oxygen content (see Glock et al., 2012 for a review), structural proxies in brachiopods have primarily concerned morphology of the calcite fibres (Ye et al., 2018, 2019), and only little information exists on brachiopod pores. Most recent brachiopod taxa, with the exception of the order Rhynchonellida, build a shell characteristic of perforations – punctae (Fig. 10). In M. venosa and other terebratellids, punctae (sensu stricto endopunctae) comprise of papillose

extensions of the mantle that link the inner epithelium with outer periostractum (Williams et al., 1997; Pérez-Huerta et al., 2009). Punctae have been proposed to function as sensory devices, storage compartments or to be involved in respiration, however, their role still remains unclear (Pérez-Huerta et al., 2009; Thayer, 1986). In an attempt to find a link between the punctae and environmental stressors we quantify the punctae volume. Although we note that further replicates are necessary before a final statement can be made, our results indicate that brachiopods both under low-pH_{sw}/Ω_{cal} conditions and particularly during thermal stress built shell with relatively more punctae volume (from ~13% at control conditions, to 17% under acidification and 24% under high temperature) than biomineral (Fig. 7, Table 3). This is also in line with microstructural investigations of Ye et al. (2019) who found that M. venosa exposed to acidification produced a shell with overall larger, and higher density of endopunctae. This suggests punctae as being valuable for evaluating structural changes in relationship to ambient stressors, and highlights the potential of punctae volume as a novel quantitate measure. Potentially, punctae volume assessment may also find application as a proxy in palaeo-environmental reconstructions. Since very distinct punctae volumes were estimated from shells grown under different conditions (i.e. normal control or natural conditions, to acidification and high temperature), it may be possible that the punctae volume itself could be indicative of the environmental conditions. Certainly, this would require further assessment evaluating the variability between individuals exposed to the same conditions, and the definition of a threshold volume value that will enable for clear separating between the different environmental conditions or stressor categories. Rather than specific environmental conditions, however, it is most likely that the increasing punctae contents with acidification and temperature reflect the degree of stress experienced, or energetic costs required for survival, as punctae have been proposed to play a role in physiological functioning. This points towards the high temperature treatment as particularly unfavourable, and temperature as being the main parameter affecting the shell formation in M. venosa, as observed by the overall reduced shell growth in terms of length and also the increased pore volume relative to calcite. An advantage of this method is that it could be relatively easily transferable to fossil brachiopods, since it is possible to quantify punctae volumes even when punctae are filled with sediment (they will have different density than the calcite shell). A potential complication could arise when punctae are infilled with calcite, however, as calcite cement will likely have a very different elemental composition (and particularly higher Mg content), it could be possible to discriminate between different calcite types. Certainly, this will depend on the diagenetic environment and awaits a more complete assessment, but could present a promising direction for future palaeo-environmental research employing brachiopods, in addition to their geochemical signatures. Finally, an interesting observation was that the punctae volume was highly comparable between an individual from nature and a specimen from the control culturing treatment, suggesting that our control conditions were representative of the natural habitat.

5. CONCLUSIONS

Our work illuminates the underlying controls on incorporation of some key elements into the brachiopod M. venosa and revisits the application of various elemental ratios as a proxy for carbonate system parameters, temperature and culture medium/seawater chemistry. The findings and interpretations from this study might also be applicable to T. dorsata, based on observed shared trends between M. venosa and T. dorsata, and potentially other brachiopod species, in particular, terebratellids. Taken together, our findings identify influences from confounding parameters on several commonly used proxies and especially those considered as temperature indicators, casting doubt on the reliability of the approach of using elemental ratios for robust palaeo-oceanographical and palaeo-environmental reconstructions. We did not find any relationship between B/Ca and carbonate system parameters and in general the partitioning coefficients for B varied greatly between the aquariums (both control and acidification treatments). Reasons for this remain unsettled, and indicate the presence of an obscured variable potentially controlling the incorporation of B that could not be resolved in this study, even despite the closely monitored system. We observed a close apparent dependency of shell Li/Ca on culture medium Ω_{cal}, which in the absence of Li/Ca data on the culture medium could be misleadingly interpreted as a proxy trend. Instead, we show that partitioning of Li is in addition strongly influenced by other factors including temperature, growth effects and/or seawater/culture medium chemical composition, complicating the use of this ratio as a diagnostic tool without thorough previous evaluation. Further, we show that Mg distribution in the brachiopod calcite is more complex than previously thought, due to the multiple influences on its incorporation including carbonate chemistry, microstructural features and growth rates. Moreover, we demonstrate that M. venosa shell formation is strongly affected by thermal stress, complicating discrimination between temperature vs. growth related effects on the incorporation of Mg. This could present a potential challenge in other calcifiers as well, as thermal stress and metabolic processes are closely linked, demanding caution during calibrations of geochemical temperature proxies. We underscore Sr as a promising elemental indicator for carbonate chemistry changes, based on the observed preferential incorporation of Sr^{2+} with increasing DIC, without apparent influences from other environmental factors. We devise the first biomineralisation model for brachiopods, which provides a simple mathematical framework for explaining the Sr/Ca, with modelled and measured trends giving a good agreement. The positive dependency of Sr partitioning as a function of DIC can be explained in terms of a decreased Ca^{2+} influx to the calcifying fluid in order to maintain homeostasis, resulting in preferential substitution of Ca^{2+} with Sr^{2+} in the crystal lattice. Similar to Sr, we observe

increased incorporation of Mg with DIC, which as a physiologically mediated element is, however, expected to be transported by distinct cation pathways and thus difficult to integrate into our model. This highlights the need for further research into biomineralisation mechanisms, which may not only reconcile the partitioning of elements, but also bring new insights into the physiological mechanisms that enable brachiopods to build their shells under strong biological control. We encourage further calibration studies focusing on Sr partitioning, considering a much wider DIC range and also other brachiopod species (especially terebratellids which appear to share common physicochemical features), which will be important for improving our calibration and validating our model. Finding a robust proxy for carbonate system parameters is highly desired, as it would reduce uncertainty on current palaeo-pH and palaeo-pCO$_2$ records. Finally, our structural analyses show that punctae volume assessment could present a novel quantitative parameter for evaluating physiological stress, and potentially the underlying environmental cause, opening a way for new direction of future research on brachiopods.

Declaration of Competing Interest

The authors declare that they have no known competing financial interests or personal relationships that could have appeared to influence the work reported in this paper.

APPENDIX A. ACTIVITY MODEL

Saturation state in brachiopod calcifying fluid (CF) was calculated from ionic activities as described in Keul et al. (2017). This model is designed for calculating the distribution coefficients for divalent cations in supersaturated CF, taking into account different activities of Ca ions in seawater/culture medium and CF. According to Langer et al. (2006) the following relation describes the partition coefficients for Sr ($K_{D(Sr)}$):

$$K_{D(Sr)} = K^0_{D(Sr)} \times \frac{\{Ca^{2+}\}_{sw}}{\{Ca^{2+}\}_{CF}}$$
$$= K^0_{D(Sr)} \times \frac{\gamma_{sw} \times [Ca^{2+}]_{sw}}{\gamma_{CF} \times [Ca^{2+}]_{CF}} \qquad (A1)$$

where the $K^0_{D(Sr)}$ is the equilibrium distribution of Sr, $\{Ca^{2+}\}_{sw}$ and $\{Ca^{2+}\}_{CF}$ represent the Ca ion activities in seawater and calcifying fluid, respectively, $[Ca^{2+}]_{sw}$ and $[Ca^{2+}]_{CF}$ describe the molar concentrations, and γ_{sw} and γ_{CF} are the activity coefficients for each. Following Keul et al. (2017) we consider γ_{sw} of 0.2 for Ca ions in seawater and γ_{CF} between 0.2 and 1 due to biological regulation of Ca in the CF.

The saturation state in CF, as previously defined, describes the ratio of the product of calcium and carbonate ions to the stoichiometric solubility product K_{sp}^*:

$$\Omega_{CF} = \frac{\{Ca^{2+}\}_{CF} \times \{CO_3^{2-}\}_{CF}}{K_s} = \frac{[Ca^{2+}]_{CF} \times [CO_3^{2-}]_{CF}}{K_{sp}^*} \quad (A2)$$

Rewriting the equation according to Ca ion concentration $[Ca^{2+}]$ gives:

$$[Ca^{2+}]_{CF} = \frac{\Omega_{CF} \times K_{sp}^*}{[CO_3^{2-}]_{CF}} \qquad (A3)$$

Assuming pH$_{CF} \approx 7.8 \approx$ constant (Jurikova et al., in press-a) and DIC$_{CF} \approx$ DIC$_{sw}$, the equilibrium distribution of carbonate and bicarbonate ions can be calculated. The factors f and g can be quantified by applying slopes from linear regression of carbonate and bicarbonate ions, giving the following relationship:

$$[CO_3^{2-}]_{CF} = f \times [HCO_3^-]_{CF} = f \times g \times [DIC]_{CF}$$
$$= h \times [DIC]_{CF} \qquad (A4)$$

By substituting the Eqs. (A3) and (A4) into Eq. (A1), the dependency of distribution coefficients on DIC may be expressed:

$$K_{D(Sr)} = K^0_{D(Sr)} \times \frac{\gamma_{sw} \times [Ca^{2+}]_{sw} \times h}{\gamma_{CF} \times \Omega_{CF} \times K_{sp}^*} \times [DIC]_{CF}$$
$$= m \times [DIC]_{CF} \qquad (A5)$$

The sum of the constant factors for the factor m describes the slope of the linear trend between the $K_{D(Sr)}$ and DIC in the CF as proposed by Keul et al. (2017):

$$m = K^0_{d(Sr)} \times \frac{\gamma_{sw} \times [Ca^{2+}]_{sw} \times h}{\gamma_{CF} \times \Omega_{CF} \times K_{sp}^*} \qquad (A6)$$

The slope value is obtained from the linear regression between the DIC and measured $K_{D(Sr)}$. Reorganising Eq. (A6) after saturation state we obtain:

$$\Omega_{CF} = K^0_{d(Sr)} \times \frac{\gamma_{sw} \times [Ca^{2+}]_{sw} \times h}{\gamma_{CF} \times m \times K_{sp}^*} \qquad (A7)$$

For calculating the equilibrium distribution coefficients we assume $\Omega_{CF} = 1$. The $[Ca^{2+}]_{sw}$ corresponds to the measured Ca concentration in seawater, and the factor h results from the equilibrium distribution of carbonate species, determined from DIC and the given pH. The stoichiometric

solubility product $K_{sp}{}^*$ was calculated following Mucci (1983). The activity coefficients $\gamma_{sw} = 0.2$ and $\gamma_{CF} = 0.2$ to 1 were considered, with $\gamma_{CF} = 0.6$ giving a supersaturated CF of $\Omega_{CF} \sim 10$ (with a calculated range of Ω_{CF} values between 9.4 and 13.8).

APPENDIX B. CALCULATION OF MODEL UNCERTAINTY ENVELOPE

The model uncertainty envelope was calculated using Gaussian error propagation:

$$\Delta y(x_i) = \sqrt{\sum \left(\left| \frac{\partial y}{\partial x_i} \right| * \Delta x_i \right)^2} \tag{B1}$$

Input parameters for error calculation	Output parameters for error calculation
Deviation Temperature	Error for K_0
Deviation Salinity	Error for K_1
Deviation pH	Error for K_2
Deviation DIC	Error for K_{sp}
Deviation saturation state in calcifying fluid	Error for H^+ concentration
Deviation trace element concentration in seawater (assumed to be equal in calcifying fluid)	Error for CO_2 concentration
Deviation of trace element-calcium-ratio in seawater	Error for HCO_3^- concentration
	Error for CO_3^{2-} concentration
	Error for Ca^{2+} concentration
	Error for partition coefficient of trace element TE

APPENDIX C. SUPPLEMENTARY MATERIAL

Supplementary data to this article can be found online at https://doi.org/10.1016/j.gca.2020.07.026.

REFERENCES

Addadi L., Raz S. and Weiner S. (2003) Taking advantage of disorder: amorphous calcium carbonate and its roles in biomineralization. *Adv. Mater.* **15**, 959–970. https://doi.org/10.1002/adma.200300381.

Allen K. A. and Hönisch B. (2012) The planktic foraminiferal B/Ca proxy for seawater carbonate chemistry: a critical evaluation. *Earth Planet. Sci. Lett.* **345–348**, 203–2011.

Allen G. J. and Sanders D. (1994) Two voltage-gated, calcium release channels coreside in the vacuolar membrane of broad bean guard cells. *The Plant Cell Online* **6**, 685–694.

Atkinson M. J. and Bingman C. (1998) Elemental composition of commercial seasalts. *J. Aquaricult. Aquat. Sci.* **7**, 39–43.

Baumgarten S., Laudien J., Jantzen C., Häussermann V. and Försterra G. (2013) Population structure, growth and production of a recent brachiopod from the Chilean fjord region. *Mar. Ecol.* **35**, 401–413.

Brand U., Posenato R., Came R., Affek H., Angiolini L., Azmy K. and Farabegoli E. (2012) The end-Permian mass extinction: a rapid volcanic CO_2 and CH_4-climatic catastrophe. *Chem. Geol.* **323**, 121–144. https://doi.org/10.1016/j.chemgeo.2012.06.015.

Brand U., Logan A., Hiller N. and Richardson J. (2003) Geochemistry of modern brachiopods: applications and implications for oceanography and paleoceanography. *Chem. Geol.* **198**, 305–334. https://doi.org/10.1016/S0009-2541(03)00032-9.

Beck J. W., Edwards R. L., Ito E., Taylor F. W., Recy J., Rougerie F., Joannot P. and Henin C. (1992) Sea-surface temperature from coral skeletal strontium/calcium ratios. *Science* **257**, 644–647.

Brečević L. and Nielsen A. E. (1989) Solubility of amorphous calcium carbonate. *J. Cryst. Growth* **98**, 503–510.

Bryan S. P. and Marchitto T. M. (2008) Mg/Ca-temperature proxy in benthic foraminifera: new calibrations from the Florida Straits and a hypothesis regarding Mg/Li. *Paleoceanography* **23**, PA2220. https://doi.org/10.1029/2007PA001553.

Buening N. and Carlson S. J. (1992) Geochemical investigation of growth in selected Recent articulate brachiopods. *Lethaia* **25**, 331–345. https://doi.org/10.1111/j.1502-3931.1992.tb01402.x.

Butler S., Bailey T. R., Lear C. H., Curry G. B., Chems L. and McDonald I. (2015) The Mg/Ca temperature relationship in brachiopod shells: calibrating a potential palaeoseasonality proxy. *Chem. Geol.* **397**, 106–117. https://doi.org/10.1016/j.chemgeo.2015.01.009.

Carpenter S. J. and Lohmann K. C. (1992) Sr/Mg ratios of modern marine calcite: empirical indicators of ocean chemistry and precipitation rate. *Geochim. Cosmochim. Acta* **56**, 1837–1849.

Case D. H., Robinson L., Auro M. E. and Gagnon A. C. (2010) Environmental and biological controls on Mg and Li in deep-sea scleractinian corals. *Earth Planet. Sci. Lett.* **300**, 215–225.

Cohen A. L. and McConnaughey T. A. (2003) Geochemical perspectives on coral mineralization. *Rev. Mineral. Geochem.* **54**, 151–187. https://doi.org/10.2113/0540151.

Cross E. L., Peck L. S. and Harper E. M. (2015) Ocean acidification does not impact shell growth or repair of the Antarctic brachiopod *Liothyrella uva* (Broderip, 1833). *J. Exp. Mar. Biol. Ecol.* **462**, 29–35.

Cross E. L., Peck L. S., Lamare M. D. and Harper E. M. (2016) No ocean acidification effects on the shell growth and repair in the New Zealand brachiopod *Calloria inconspicua* (Sowerby, 1846). *J. Mar. Sci.* **73**, 920–926. https://doi.org/10.1093/icesjms/fsv031.

Cusack M., Pérez-Huerta A., Janousch M. and Finch A. A. (2008) Magnesium in the lattice of calcite shelled brachiopods. *Chem. Geol.* **257**, 59–64. https://doi.org/10.1016/j.chemgeo.2008.08.007.

de Nooijer L. J., Brombacher A., Mewes A., Langer G., Nehrke G., Bijma J. and Reichart G.-J. (2017) Ba incorporation in benthic foraminifera. *Biogeosciences* **14**, 3387–3400.

DeCarlo T. M., D'Olivo J. P., Foster T., Holcomb M., Becker T. and McCulloch M. T. (2017) Coral calcifying fluid aragonite saturation stated derived from Raman spectroscopy. *Biogeosciences* **14**, 5253–5269. https://doi.org/10.5194/bg-14-5253-2017.

Delaney M. L., Popp B. N., Lepzelter C. G. and Anderson T. F. (1989) Lithium-to-calcium ratios in modern, Cenozoic and Paleozoic articulate brachiopod shells. *Paleoceanography* **4**, 681–691. https://doi.org/10.1029/PA004i006p00681.

Dellinger M. et al. (2018) The Li isotope composition of marine biogenic carbonates: patterns and mechanisms. *Geochim. Cosmochim. Acta* **236**, 315–335.

Doss W., Marchitto T. M., Eagle R., Rashid H. and Tripati A. (2018) Deconvolving the saturation state and temperature controls on benthic foraminiferal Li/Ca, based on downcore

paired B/Ca measurements and coretop compilation. *Geochim. Cosmochim. Acta* **236**, 297–314. https://doi.org/10.1016/j.gca.2018.02.029.

Douville E., Paterne M., Cabioch G., Louvat P., Gaillardet J., Juillet-Leclerc A. and Ayliffe L. (2010) Abrupt sea surface pH change at the end of the Younger Dryas in the central sub-equatorial Pacific inferred from boron isotope abundance in corals (*Porites*). *Biogeosciences* **7**, 2445–2459.

England J., Cusack M. and Lee M. R. (2006) Magnesium and sulphur in the calcite shells of two brachiopods, *Terebratulina retusa* and *Novocrania anomala*. *Lethaia* **40**, 2–10. https://doi.org/10.1111/j.1502-3931.2006.00001.x.

Erez J. (2003) The source of ions for biomineralization in foraminifera and their implications for paleoceanographic proxies. *Rev. Mineral. Geochem.* **54**, 115–149.

Farkaš J., Böhm F., Wallmann K., Blenkinsop J., Eisenhauer A., van Geldern R., Munecke A., Voigt S. and Veizer J. (2007) Calcium isotope record of Phanerozoic oceans: implications for chemical evolution of seawater and its causative mechanisms. *Geochim. Cosmochim. Acta* **71**, 5117–5134.

Finch A. A. and Allison N. (2007) Coordination of Sr and Mg in calcite and aragonite. *Mineral. Mag.* **7**, 539–552.

Fowell S. E., Sandford K., Stewart J. A., Castillo K. D., Ries J. B. and Foster G. L. (2016) Intrareef variation in Li/Mg and Sr/Ca sea surface temperature proxies in the Caribbean reef-building coral *Siderastrea siderea*. *Paleoceanography* **31**, 1315–1329. https://doi.org/10.1002/2016PA002968.

Füger A., Konrad F., Leis A., Dietzel M. and Mavromatis V. (2019) Effect of growth rate and pH on lithium incorporation in calcite. *Geochim. Cosmochim. Acta* **248**, 14–24. https://doi.org/10.1016/j.gca.2018.12.040.

Gabitov R. I., Sadekov A. and Leinweber A. (2014) Crystal growth rate effect on Mg/Ca and Sr/Ca partitioning between calcite and fluid: an *in situ* approach. *Chem. Geol.* **367**, 70–82. https://doi.org/10.1016/j.chemgeo.2013.12.019.

Garbelli C., Shen S.-Z., Immenhauser A., Brand U., Buhl D., Wang W. Q., Zhang H. and Shi G. R. (2019) Timing of Early and Middle Permian deglaciation of the southern hemisphere: brachiopod-based ^{87}Sr/^{86}Sr calibration. *Earth Planet Sci. Lett.* **516**, 122–135. https://doi.org/10.1016/j.epsl.2019.03.039.

Garbelli C., Angiolini L. and Shen S.-Z. (2017) Biomineralization and global change: a new perspective for understanding the end-Permian extinction. *Geology* **45**, 19–22.

Gaspard D., Aldridge A. E., Boudouma O., Fialin M., Rividi N. and Lécuyer C. (2018) Analysis of growth and form in *Aerothyris kerguelenensis* (rhynchonelliform brachiopod) – Shell spiral devaitions, microstructure, trace element contents and stable isotopes. *Chem. Geol.* **483**, 474–490.

Glock N., Schönfeld J. and Mallon J. (2012) The functionality of pores in benthic Foraminifera and bottom water oxygenation: a review. In: ANOXIA: Evidence for Eukaryote Survival and Paleontological Strategies, Cellular Origin, Life in Extreme Habitats and Astrobiology (eds. A. V. Altenbach, J. M. Bernhard and J. Seckbach), Vol. 21. Springer, pp. 540–556.

Glock N., Erdem Z., Wallmann K., Somes C. J., Liebetrau V., Schönfeld J., Gorb S. and Eisenhauer A. (2018) Coupling of oceanic carbon and nitrogen facilitates spatially resolved quantitative reconstruction of nitrate inventories. *Nat. Comm.* **9**, 1217.

Griesshaber E., Kelm K., Sehrbrock A., Mader W., Mutterlose J., Brand U. and Schmahl W. (2009) Amorphous calcium carbonate in the shell material of the brachiopod *Megerlia truncata*. *Eur. J. Mineral* **21**, 715–723.

Guo W. (2019) Seawater temperature and buffering capacity modulate coral calcifying fluid. *Sci. Rep.* **9**, 1189.

Hathorne E. C., Felis T., Suzuki A., Kawahata H. and Cabioch G. (2013a) Lithium in the aragonite skeletons of massive *Porites* corals: a new tool to reconstruct tropical sea surface temperatures. *Paleoceanography* **28**, 143–152. https://doi.org/10.1029/2012PA002311.

Hathorne et al. (2013b) Interlaboratory study for coral Sr/Ca and other element/Ca ratio measurements. *Geochem. Geophys. Geosys.* **14**. https://doi.org/10.1002/ggge.20230.

Hemming N. G., Reeder R. J. and Hanson G. N. (1995) Mineral-fluid partitioning and isotopic fractionation of boron in synthetic calcium carbonate. *Geochim. Cosmochim. Acta* **59**, 371–379.

Henehan M. J., Foster G. L., Rae J. W. B., Prentice K. C., Erez J., Bostock H. C., Marshall B. J. and Wilson P. A. (2015) Evaluating the utility of B/Ca ratios in planktic foraminifera as a proxy for the carbonate system: a case study of *Globigerinoides ruber*. *Geochem. Geophys. Geosyst.* **16**, 1052–1069. https://doi.org/10.1002/2014GC005514.

Jurikova H., Liebetrau V., Gutjahr M., Rollion-Bard C., Hu M. Y., Krause S., Henkel D., Hiebenthal C., Schmidt M., Laudien J. and Eisenhauer A. (in press-a) Boron isotope systematics of cultured brachiopod calcite: response to acidification, vital effects and implications for palaeo-pH reconstruction. *Geochim. Cosmochim. Acta* **248**, 370–386.

Jurikova H., Liebetrau V., Raddatz J., Fietzke J., Trotter J., Rocholl A., Krause S., McCulloch M., Rüggeberg A. and Eisenhauer A. (in press-b) Boron isotope composition of the cold-water coral *Lophelia pertusa* along the Norwegian margin: zooming into a potential pH-proxy by combining bulk and high-resolution approaches. *Geochim. Cosmochim. Acta* **248**, 370–386. https://doi.org/10.1016/j.chemgeo.2019.01.005, in press.

Keul N., Langer G., Thoms S., de Nooijer L. J., Reichart G.-J. and Bijma J. (2017) Exploring foraminiferal Sr/Ca as a new carbonate system proxy. *Geochim. Cosmochim. Acta* **202**, 374–386.

Kocsis L., Dulai A., Cipriani A., Vennemann T. and Yunsi M. (2020) Geochemistry of recent and fossil brachiopod calcite of *Megathiris detruncata* (Terebratulida, Megathyrididae): a modern baseline study to trace past environmental conditions. *Chem. Geol.* **533** 119335.

Langer G., Sadekov A., Nehrke G., Baggini C., Rodolfo-Metalpa R., Hall-Spencer J. M., Cuoco E., Bijma J. and Elderfield H. (2018) Relationship between mineralogy and minor element partitioning in limpets from an Ischia CO_2 vent site provides new insights into their biomineralization pathway. *Geochim. Cosmochim. Acta* **236**, 218–229.

Langer G., Gussone N., Nehrke G., Riebesell U., Eisenhauer A., Kuhnert H., Rost B., Trimborn S. and Thoms S. (2006) Coccolith strontium to calcium ratios in *Emiliania huxleyi*: The dependence on seawater strontium and calcium concentrations. *Limnol. Oceanogr.* **51**, 310–320.

Lear C. H., Mawbey E. M. and Rosenthal Y. (2010) Cenozoic benthic foraminiferal Mg/Ca and Li/Ca records: toward unlocking temperatures and saturation states. *Paleoceanography* **25**, PA4215. https://doi.org/10.1029/2009PA001880.

Lécuyer C., Grandjean P., Reynard B., Albarède F. and Telouk P. (2002) ^{11}B/^{10}B analysis of geological materials by ICP-MS Plasma 54: application to the boron fractionation between brachiopod calcite and seawater. *Chem. Geol.* **186**, 45–55.

Marriott C. S., Henderson G. M., Crompton R., Staubwasser M. and Shaw S. (2004a) Effect of mineralogy, salinity, and temperature on Li/Ca and Li isotope composition of calcium carbonate. *Chem. Geol.* **212**(1–2), 5–15. https://doi.org/10.1016/j.chemgeo.2004.08.002.

Marriott C. S., Henderson G. M., Belshaw N. S. and Tudhope A. W. (2004b) Temperature dependence of δ^7Li, δ^{44}Ca and Li/Ca during growth of calcium carbonate. *Earth Planet. Sci. Lett.* **222**(2), 615–624. https://doi.org/10.1016/j.epsl.2004.02.031.

Marshall A. T. (1996) Calcification in hermatypic and ahermatypic corals. *Science* **271**, 637–639.

Mass T., Giuffre A. J., Sun C.-Y., Stifler C. A., Frazier M. J., Neder M., Tamura N., Stan C. V., Marcus M. A. and Gilbert P. U. P. A. (2017) Amorphous calcium carbonate particles form coral skeletons. *Proc. Natl. Acad. Sci.* **28**, E7670–E7678.

McCulloch M., Trotter J., Montagna P., Falter J., Dunbar R., Freiwald A., Försterra G., López Correa M., Maier C., Rüggeberg A. and Taviani M. (2012) Resilience of cold-water scleractinian corals to ocean acidification: boron isotopic systematics of pH and saturation state up-regulation. *Geochim. Cosmochim. Acta* **87**, 21–34. https://doi.org/10.1016/j.gca.2012.03.

Mezger E. M., de Nooijer L. J., Boer W., Brummer G. J. A. and Reichart G. J. (2016) Salinity controls on Na incorporation in Red Sea planktonic foraminifera. *Paleoceanography* **31**, 1562–1582.

Mitsuguchi T., Matsumoto E., Abe O., Uchida T. and Isdale P. J. (1996) Mg/Ca thermometry in coral skeletons. *Science* **274**, 961–963.

Montagna P. et al. (2014) Li/Mg systematics in scleractinian corals: calibration of the thermometer. *Geochim. Cosmochim. Acta* **132**, 288–310.

Mucci A. (1983) The solubility of calcite and aragonite in seawater at various salinities, temperatures, and one atmosphere total pressure. *Am. J. Sci.* **283**, 780–799.

Müller M. N., Lebrato M., Riebesell U., Barcelos e Ramos J., Schulz K. G., Blanco-Ameijeiras S., Sett S., Eisenhauer A. and Stoll H. M. (2014). *Influence of temperature and CO$_2$ on the strontium and magnesium composition of coccolithophore calcite, Biogeosciences* **11**, 1065–1075.

Nadler M. J. S., Hermosura M. C., Inabe K., Perraud A.-L., Zhu Q., Stokes A. J., Kurosaki T., Kinet J.-P., Penner R., Scharenberg A. M. and Fleig A. (2001) LTRPC7 is a Mg ATP-regulated divalent cation channel required for cell viability. *Nature* **411**, 590–595.

Nehrke G., Keul N., Langer G., de Nooijer L. J., Bijma J. and Meibom A. (2013) A new model for biomineralization and trace-element signatures of foraminifera tests. *Biogeosciences* **10**, 6759–6767. https://doi.org/10.5194/bg-10-6759-2013.

Nürnberg D., Bijma J. and Hemleben C. (1996) Assessing the reliability of magnesium in foraminiferal calcite as a proxy for water mass temperature. *Geochim. Cosmochim. Acta* **60**, 803–814.

Okai T., Suzuki A., Kawahata H., Terashima S. and Imai N. (2002) Preparation of a new geological survey of Japan geochemical reference material: coral JCp-1. *Geostand. Geoanal. Res.* **26**, 95–99.

Penman D. E., Hönisch B., Rasbury E. T., Hemming N. G. and Spero H. J. (2013) Boron, carbon, and oxygen isotopic composition of brachiopod shells: Intra-shell variability, controls, and potential as a paleo-pH recorder. *Chem. Geol.* **340**, 32–39.

Pérez-Huerta A., Cusack M., Jeffries T. E. and Williams C. T. (2008) High resolution distribution of magnesium and strontium and the evaluation of Mg/Ca thermometry in recent brachiopod shells. *Chem. Geol.* **247**, 229–241.

Pérez-Huerta A., Cusack M., McDonald S., Marone F., Stampanoni M. and MacKay S. (2009) Brachiopod punctae: a complexity in shell biomineralisation. *J. Struct. Biol.* **167**, 62–67.

Politi Y., Metzler R. A., Abrecht M., Gilbert B., Wilt F. H., Sagi I., Addadi L., Weiner S. and Gilbert P. U. (2008) Transformation mechanism of amorphous calcium carbonate into calcite in the sea urchin larval spicule. *Proc. Natl. Acad. Sci.* **105**, 17362–17366.

Powell M. G., Schöne B. R. and Jacob D. E. (2009) Tropical marine climate during the late Paleozoic ice age using trace element analyses of brachiopods. *Palaeogeogr. Palaeoclimatol. Palaeoecol.* **280**, 143–149. https://doi.org/10.1016/j.palaeo.2009.06.003.

Raddatz J., Liebetrau V., Rüggeberg A., Hathorne E., Krabbenhöft A., Eisenhauer A., Böhm F., Vollstaedt H., Fietzke J., Lòpez Correa M., Freiwald A. and Dullo W.-C. (2013) Stable Sr-isotope, Sr/Ca, Mg/Ca/Li/Ca and Mg/Li ratios in the scleractinian cold-water coral *Lophelia pertusa. Chem. Geol.* **352**, 143–152.

Rae J. W. B., Foster G. L., Schmidt D. N. and Elliott T. (2011) Boron isotopes and B/Ca in benthic foraminifera: proxies for the deep ocean carbonate system. *Earth Planet. Sci. Lett.* **302**, 403–413.

Raitzsch M., Dueñas-Bohórquez A., Reichart G.-J., de Nooijer L. J. and Bickert T. (2010) Incorporation of Mg and Sr in calcite of cultured benthic foraminifera: impact of calcium concentration and associated calcite saturation state. *Biogeosciences* **7**, 869–881. https://doi.org/10.5194/bg-7-869-2010.

Roberts J., Kaczmarek K., Langer G., Skinner L. C., Bijma J., Bradbury H., Turchyn A. V., Lamy F. and Misra S. (2018) Lithium isotopic composition of benthic foraminifera: a new proxy for paleo-pH reconstruction. *Geochim. Cosmochim. Acta* **236**, 336–350. https://doi.org/10.1016/j.gca.2018.02.038.

Roda M. S., Griesshaber E., Ziegler A., Rupp U., Yin X., Henkel D., Häussermann V., Laudien J., Brand U., Eisenhauer A., Checa A. G. and Schmahl W. W. (2019) Calcite fibre formation in modern brachiopod shells. *Sci. Rep.* **9**, 598.

Rollion-Bard C., Milner García S., Burckel P., Angiolini L., Jurikova H., Tomašových A. and Henkel D. (2019) Assessing the biomineralization processes in the shell layers of modern brachiopods from oxygen isotopic composition and elemental ratios: implication for their use as paleoenvironmental proxies. *Chem. Geol.* **524**, 49–66. https://doi.org/10.1016/j.chemgeo.2019.05.031.

Romanin M., Crippa G., Ye F., Brand U., Bitner M. A., Gaspard D., Häussermann V. and Laudien J. (2018) A sampling strategy for recent and fossil brachiopods: selecting the optimal shell segment for geochemical analyses. *Riv. Ital. Paleontol. S.* **124**, 343–359.

Russell A. D., Hönisch B., Spero H. J. and Lea D. W. (2004) Effects of seawater carbonate ion concentration and temperature on shell U, Mg, and Sr in cultured planktonic foraminifera. *Geochim. Cosmochim. Acta* **68**, 4347–4361. https://doi.org/10.1016/j.gca.2004.03.013.

Roy R. N., Roy L. N., Vogel K. M., Porter-Moore C., Pearson T., Good C. E., Millero F. J. and Campbell D. M. (1993) The dissociation constant of carbonic acid in seawater at salinities 5 to 45 and temperatures 0 to 45 °C. *Mar. Chem.* **44**, 249–267.

Schmahl W. W., Griesshaber E., Neuser R., Lenze A., Job R. and Brand U. (2004) The microstructure of the fibrous layer of terebratulide brachiopod shell calcite. *Eur. J. Mineral* **16**, 693–697.

Sevilgen D. S., Venn A. A., Hu M. Y., Tambutté E., de Beer D., Planas-Bielsa V. and Tambutté (2019) Full *in vivo* characterisation of carbonate chemistry at the site of calcification. *Sci. Adv.* **5**, eaau7447.

Tanaka K., Okaniwa N., Miyaji T., Murakami-Sugihara N., Zhao L., Tanabe K., Schöne B. R. and Shirai K. (2019) Microscale

magnesium distribution in shell of Mediterranean mussel *Mytilus galloprovincialis*: an example of multiple factors controlling Mg/Ca in biogenic calcite. *Chem. Geol.* **511**, 521–523. https://doi.org/10.1016/j.chemgeo.2018.10.025.

Tang J., Köhler S. J. and Dietzel M. (2008) Sr^{2+}/Ca^{2+} and $^{44}Ca/^{40}Ca$ fractionation during inorganic calcite formation: I. Sr incorporation. *Geochim. Cosmochim. Acta* **72**, 3718–3732.

Taylor A. R., Chrachri A., Wheeler G., Goddard H. and Brownlee C. (2011) A Voltage-Gated H^+ Channel Underlying pH Homeostasis in Calcifying Coccolithophores. *PLoS Biol* **9**. https://doi.org/10.1371/journal.pbio.1001085 e1001085.

Thayer C. W. (1986) Respiration and the function of brachiopod punctae. *Lethaia* **19**, 23–31.

Ullmann C. V., Frei R., Korte C. and Lüter C. (2017) Element/Ca, C and O isotope ratios in modern brachiopods: species-specific signals of biomineralization. *Chem Geol.* **460**, 15–24.

Ullmann C. V. and Pogge von Strandmann P. A. E. (2017) The effect of shell secretion rate on Mg/Ca and Sr/Ca ratios in biogenic calcite as observed in a belemnite rostrum. *Biogeosciences* **14**, 89–97.

Veis A. (2003) Mineralization in organic matrix frameworks. *Rev. Mineral Geochem.* **54**, 249–289.

Veizer J., Ala D., Azmy K., Bruckschen P., Buhl D., Bruhn F., Carden G. A. F., Diener A., Ebneth S., Godderis Y., Jasper T., Korte C., Pawellek F., Podlaha O. G. and Strauss H. (1999) $^{87}Sr/^{86}Sr$, $\delta^{13}C$ and $\delta^{18}O$ evolution of Phanerozoic seawater. *Chem. Geol.* **161**, 59–88.

Vigier N., Rollion-Bard C., Levenson Y. and Erez J. (2015) Lithium isotopes in foraminifera shells as a novel proxy for the ocean dissolved inorganic carbon (DIC). *C. R. Geosci.* **347**, 43–51.

Vollstaedt H., Eisenhauer A., Wallmann K., Böhm F., Fietzke J., Liebetrau V., Krabbenhöft A., Farkaš J., Tomašovych A., Raddatz J. and Veizer J. (2014) The Phanerozoic $\delta^{88/86}Sr$ record of seawater: new constraints on past changes in oceanic carbonate fluxes. *Geochim. Cosmochim. Acta* **128**, 249–265.

Weiss R. F. (1974) Carbon dioxide in water and seawater: the solubility of a non-ideal gas. *Mar. Chem.* **2**, 203–215.

Williams A., Brunton C. H. C. and MacKinnon D. I. (1997) Morphology. In *Treatise on Invertebrate Paleontology Part H Brachiopoda* (ed. R. L. Kaesler). The Geological Society of America and The University of Kansas Press, Boulder and Lawrence, pp. 321–422.

Ye F., Crippa G., Angiolini L., Brand U., Capitani G., Cusack M., Garbelli C., Griesshaber E., Harper E. and Schmahl W. (2018) Mapping of recent brachiopod microstructure: a tool for environmental studies. *J. Struct. Biol.* **201**, 221–236. https://doi.org/10.1016/j.jsb.2017.11.011.

Ye F., Jurikova H., Angiolini A., Brand U., Crippa G., Henkel D., Laudien J., Hiebenthal C. and Šmajgl D. (2019) Variation in brachiopod microstructure and isotope geochemistry under low-pH – ocean acidification conditions. *Biogeosciences* **16**, 1–26.

Yu J. and Elderfield H. (2007) Benthic foraminiferal B/Ca ratios reflect deep water carbonate saturation state. *Earth Planet. Sci. Lett.* **258**, 73–86.

Yu J., Elderfield H. and Hönisch B. (2007) B/Ca in planktonic foraminifera as a proxy for surface seawater pH. *Paleoceanography* **22**, PA2202.

Zeebe R. E. and Wolf-Gladrow D. A. (2001) CO2 in seawater: Equilibrium, kinetics, isotopes. Elsevier Oceanography Series 65, Elsevier, 346 pages.

Zeebe R. E. and Sanyal A. (2002) Comparison of two potential strategies of plaktonic foraminifera for house building: Mg^{2+} or H^+ removal? *Geochim. Cosmochim. Acta* **66**, 1159–1169.

Zoccola D., Tambutté E., Sénégas-Balas F., Michiels J. F., Failla J. P., Jaubert J. and Allemand D. (1999) Cloning of a calcium channel alpha1 subunit from the reef-building coral, *Stylophora pistillata*. *Gene* **227**, 157–167.

Associate editor: Thomas M. Marchitto